Immunology and Inflammation
Microbiology and Infectious Disease

Reviewed Preprint
v2 • February 6, 2025
Revised by authors

Reviewed Preprint
v1 • August 14, 2024

Soluble immune mediators orchestrate protective *in vitro* granulomatous responses across *Mycobacterium tuberculosis* complex lineages

Ainhoa Arbués, Sarah Schmidiger, Miriam Reinhard, Sònia Borrell, Sébastien Gagneux, Damien Portevin

Swiss Tropical and Public Health Institute, Allschwil, Switzerland • University of Basel, Basel, Switzerland

eLife Assessment

This study describes the impact of mycobacterial genetic diversity on host-infection phenotypes by assessing the effect of different M. tuberculosis lineages on granulomatous inflammation using a 3D in vitro granuloma model. Despite being descriptive and showing mostly correlative relationships, the **useful** findings and data provide some **solid** support regarding the functional impact of M. tuberculosis natural diversity on host-pathogen interactions. The study will interest researchers working on mycobacteria and how genetic diversity influences virulence and immunity outcomes.

https://doi.org/10.7554/eLife.99062.2.sa3

Abstract

The members of the *Mycobacterium tuberculosis* complex (MTBC) causing human tuberculosis comprise ten phylogenetic lineages that differ in their geographical distribution. The human consequences of this phylogenetic diversity remain poorly understood. Here, we assessed the phenotypic properties at the host-pathogen interface of 14 clinical strains representing five major MTBC lineages. Using a human *in vitro* granuloma model combined with bacterial load assessment, microscopy, flow cytometry, and multiplexed-bead arrays, we observed considerable intra-lineage diversity. Yet, modern lineages were overall associated with increased growth rate and more pronounced granulomatous responses. MTBC lineages exhibited distinct propensities to accumulate triglyceride lipid droplets —a phenotype associated with dormancy— that was particularly pronounced in lineage 2 and reduced in lineage 3 strains. The most favorable granuloma responses were associated with strong CD4 and CD8 T cell activation as well as inflammatory responses mediated by CXCL9, granzyme B and TNF-α. Both of which showed consistent negative correlation with bacterial proliferation across genetically distant MTBC strains of different lineages. Taken together, our data

indicate that different virulence strategies and protective immune traits associate with MTBC genetic diversity at lineage and strain level.

Introduction

With an estimated 1.3 million deaths in 2022, tuberculosis (TB) remains one of the deadliest infectious diseases in the world (WHO, 2023). The main etiological agents of TB are a group of closely related bacteria collectively known as the *Mycobacterium tuberculosis* complex (MTBC). Human-adapted MTBC strains are classified into ten phylogenetic lineages (L1 to L10), which are considered "ancestral" (L1 and L5 to L10) or "modern" (L2 to L4) based on the presence or absence of the TbD1 genomic region (Brosch et al., 2002; Comas et al., 2013; Coscolla et al., 2021; Guyeux et al., 2024). Among these lineages, L1 to L4 are responsible for most of the TB cases worldwide; with less prevalent lineages restricted to specific African regions. Local adaptation to specific human hosts has been proposed to support this uneven phylogeographic distribution and disease burden of different MTBC lineages (Gagneux et al., 2006). Irrespective of the underlying reason for this phylogeographic population structure, the clinical implications of MTBC genetic diversity, particularly on vaccine efficacy, remains unclear (Perez et al., 2020).

Clinical and epidemiological studies have suggested that MTBC strains might contribute differently to disease presentation and transmissibility; with the difference between ancestral and modern lineages being particularly marked. For example, several reports have described an association between ancestral L1 and higher rates of extrapulmonary TB (Caws et al., 2008; Click et al., 2012; Saelens et al., 2022; Seraphin et al., 2017). Moreover, strains belonging to ancestral lineages display a lower capacity to transmit compared to strains from the modern lineages L2 and L4 (Caws et al., 2008; Guerra-Assuncao et al., 2015; Nebenzahl-Guimaraes et al., 2015). However, these measures of virulence are influenced by non-bacterial factors, such as host genetics and immune competency or delays in health care seeking or access. The first experimental clues regarding the phenotypic consequences of strain genetic variation in the MTBC date from the 1960s with the observation that South Indian isolates were less virulent than strains from British patients in the guinea pig model (Mitchison et al., 1960). Since then, much of our knowledge on the implications of MTBC diversity came from studies characterizing outbreak-causing strains (Manca et al., 1999; Manca et al., 2001; Newton et al., 2006), or focusing on only a few representative strains of specific lineages (Hiza et al., 2023; Romagnoli et al., 2018). However, extrapolation of strain-specific characteristics to an entire lineage can be misleading due to considerable intra-lineage heterogeneity in experimental outcomes (Portevin et al., 2011; Reiling et al., 2013; Wang et al., 2010). Furthermore, even though awareness of strain variation and its consequences is raising, the majority of immunological studies are based on laboratory-adapted reference strains such as H37Rv or Erdman. In addition, our understanding of immune protective traits in TB remains insufficient to identify good correlates of protection for the assessment of vaccines (Wang et al., 2024). In addition, the TB immunology field tends to be dominated by data from mouse and non-human primate studies, yet other *in vivo* and *in vitro* models have provided numerous valuable insights (Esaulova et al., 2021; Gideon et al., 2022; Moreira-Teixeira et al., 2020; Plumlee et al., 2021; Tezera et al., 2020; Thacker et al., 2020).

We previously demonstrated the clinical relevance of a three-dimensional (3D) *in vitro* granuloma model by mechanistically dissecting the differential resuscitation of MTB in granulomas exposed to distinct TNF-α antagonists (Arbues et al., 2020a). In this study, we aimed to extend this *in vitro* granuloma model to the study of a large collection of well-characterized and genetically diverse representatives of the MTBC (Borrell et al., 2019). We assessed bacterial virulence in terms of growth rate and characterized the individual immune responses to the various MTBC strains. Our results reveal a broad spectrum of granulomatous responses that correlate with the level of mycobacterial proliferation. Overall, strains of the modern lineages are associated with higher growth rates that correlate with increased macrophage cell death and granuloma scores (based on

size and shape); nevertheless, we also report substantial intra-lineage heterogeneity. Furthermore, our results show that granulomatous responses associated with the least replicating strains harbor an increased CD4 and CD8 T cell activation as well as the release of specific soluble factors encompassing CXCL9, granzyme B and TNF-α.

Results

Mycobacterial growth in human *in vitro* granulomas shows marked intra-lineage diversity and is overall increased for MTBC modern lineages

We selected 14 isolates (**Table 1**) from a reference set of clinical strains covering much of the global diversity of the human-adapted MTBC (Borrell et al., 2019). As a first measure of virulence, we evaluated the capacity of the strains to proliferate within 3D *in vitro* granulomas. Bacterial load based on colony forming units (CFU) was quantified on days one and eight post-infection (**Figure 1—figure supplement 1**) and used to determine the growth rate between these time points. The different strains proliferated with rates ranging from 8.1 to 136.0 (**Figure 1**). Modern lineages (L2 to L4) proliferated significantly more than ancestral ones (L1 and L5) did (median rates 52.1 [modern] vs. 27.2 [ancestral]) (**Figure 1A**). Stratification of the data by lineage revealed that the growth rate of L2 tended to be higher than that of the other modern lineages (median rates 76.0 [L2] vs. 45.1 [L3] and 53.7 [L4]) (**Figure 1B**). Nevertheless, substantial intra-lineage heterogeneity could be observed, particularly within L1 and L2 (coefficients of variation 84.4% [L1] and 66.0% [L2] vs. 32.6% [L3], 34.6% [L4] and 31.9% [L5]). As depicted in **Figure 1C**, the lower virulence observed for ancestral lineages in general was contrasted by strain L1B that displayed a high growth rate (median 64.7) comparable to that of most strains belonging to modern lineages. Moreover, while L2 Beijing strains (L2B and L2C) exhibited a characteristic hyper-virulent phenotype (median rates 76.0 and 111.6, respectively), the proto-Beijing L2A was one of the most attenuated strains (median 14.7). In comparison, L3 to L5 representative strains behaved more homogeneously. Noteworthy, the reference strain H37Rv, belonging to L4, displayed a lower growth rate than any of the evaluated L4 clinical isolates. Taken together, our results confirm the higher virulence propensities of strains from modern lineages, and L2 Beijing strains in particular, although they also highlight considerable intra-lineage diversity.

Propensity to enter dormancy is particularly pronounced in lineage 2 and reduced in lineage 3 strains

MTBC pathogenicity relies on its ability to survive the hostile and hypoxic granulomatous environment. The transcription factor DosR orchestrates the adaptation to oxygen limitation by inducing a metabolic switch into a dormant state (Garton et al., 2008; Gengenbacher and Kaufmann, 2012). A constitutive over-expression of *dosR* in L2 Beijing strains has been proposed to contribute to their enhanced virulence and transmissibility (Reed et al., 2007). A genomic duplication including the DosR operon and a synonymous SNP within Rv3134c, which generates an alternative transcriptional start site, have been linked to this increased expression of the DosR regulon (Domenech et al., 2010; Domenech et al., 2017). A hallmark of our *in vitro* granuloma model resides in the generation of a hypoxic environment leading to dormant-like MTBC features such as the loss of acid-fastness and accumulation of triacylglycerides, which can be quantified by differential Auramine-O (Au)/Nile red (NR) fluorescent staining (Arbues et al., 2020a; Arbues et al., 2021). We assessed whether MTBC genetic diversity would result in a differential propensity to enter dormancy when facing a hypoxic environment. Therefore, we quantified the ratio between dormant (Au^{-} NR^{+}) and metabolically active (Au^{+} NR^{-}) bacteria (hereafter referred to as 'dormancy ratio') for each MTBC strain (**Figure 2A** and **Figure 2—figure supplement 1A**).

Figure 1.

Mycobacterial growth in human *in vitro* granulomas shows marked intra-lineage diversity and is overall increased for MTBC modern lineages.

Growth rate between days 1 and 8 post-infection stratified by **(A)** ancestral or modern lineage, **(B)** specific lineage, or **(C)** individual strain. Colors indicate lineage and horizontal lines and bars represent medians. Shapes stand for (**A-B**) individual strains within the same lineage (LXA in circles, LXB in squares and LXC in triangles), or (**C**) independent donors (n = 4). Statistical analyses by (**A**) two-tailed Mann-Whitney, (**B**) Kruskal-Wallis or (**C**) Friedman tests with *post hoc* Dunn's correction. #, $p < 0.1$; *, $p < 0.05$; **, $p < 0.01$; ***, $p < 0.001$.

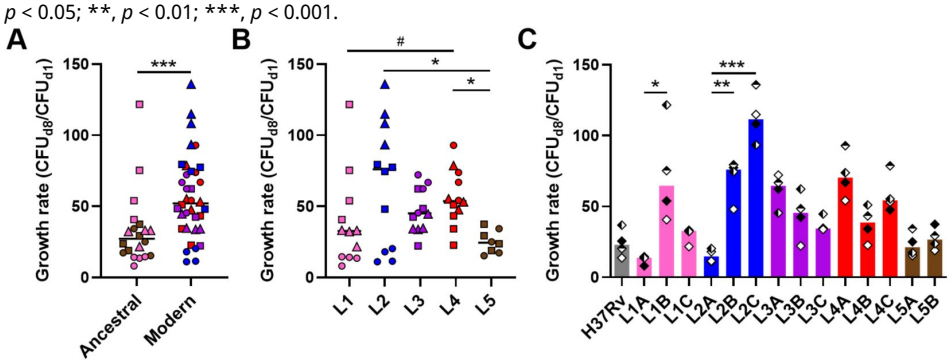

Table 1.

MTBC isolates used in this work

Strain[a]		Sublineage[b]	Patient origin	Additional information
L1A	**N0069**	L1.1.1	China	
L1B	**N0072**	L1.1.2	India	
L1C	**N0157**	L.1.2.1	Philippines	
L2A	**N0031**	L2.1	China	Proto-Beijing (DRD105, RD207 present)
L2B	**N0052**	L.2.2.2	China	Ancestral Beijing (DRD105, DRD207)
L2C	**N0155**	L2.2.1	China	Modern Beijing (DRD105, DRD207, DRD181)
L3A	**N0004**	L3.1	India	
L3B	**N0054**	ND	Ethiopia	
L3C	**N1274**	L3.2	Afghanistan	
L4A	**N1216**	L4.6.2.2	Ghana	Cameroon – "Specialist"
L4B	**N0136**	L4.3.3	USA	LAM – "Generalist"
L4C	**N1283**	L4.2.1	Germany	Ural
L5A	**N1268**	L5.1	Sierra Leone	
L5B	**N1272**	L5.1.2	Ghana	

[a] Nomenclature used in the current study (left) and in (Borrell et al., 2019) (right). [b] Classification based on (Ates et al., 2018; Coll et al., 2014; Napier et al., 2020). ND, not determined; Δ, deletion; RD, region of difference.

While approximately 50% of H37Rv bacilli acquired dormant-like features (median dormancy ratio 0.94), MTBC clinical strains showed a level of dormancy induction spanning from 0.29 to 1.98. Upon grouping strains by lineage (**Figure 2B**) and **Figure 2—figure supplement 1B**), no significant difference was found between L1, L4 and L5 (median dormancy ratios 0.85 [L1], 0.86 [L4], and 1.06 [L5]). Nonetheless, L2 strains exhibited an increased propensity to accumulate triacylglycerides (median dormancy ratio 1.30; $p = 0.072$ vs. L1 and $p < 0.05$ vs. L4 by corrected Dunn's multiple comparisons test). This result is in line with the fact that they are carriers of the aforementioned genomic events: the duplication in L2A, the Rv3134c SNP in L2B, and both in L2B. By contrast, L3 bacilli seemed more prone to remain in a metabolically active state in comparison to bacteria belonging to the other lineages (median dormancy ratio 0.54; $p = 0.072$ vs. L5 by corrected Dunn's multiple comparisons test). Interestingly, the ratio between dormant and metabolically active bacilli showed no correlation with the respective growth rate of the individual MTBC strains (**Figure 2C**). This finding suggests that an increased tendency to remain in a metabolically active state is not necessarily associated with a more pronounced growth phenotype. Further studies are necessary to better understand the dormancy ratio-growth rate relationship, and to assess how this might relate to *in vivo* virulence.

MTBC strain diversity translates into a spectrum of granulomatous responses that correlates with bacterial growth and induction of macrophage apoptosis

We next investigated the impact of MTBC strain diversity on the host immune responses within *in vitro* granulomas. We monitored cellular aggregation by bright field microscopy imaging on day seven post-infection and quantified the area and aspect ratio of the individual aggregates as well as their total number. While uninfected (UI) PBMCs did not lead to significant aggregation, all MTBC strains induced the formation of *in vitro* granulomas in variable numbers, shapes and sizes (**Figure 3A**). Despite notable donor-to-donor variability, the differential granulomatous responses induced by the individual strains were consistent across all donors (**Figure 3—figure supplement 1**). Overall, 10 to 58 *in vitro* granulomas were identified per field (**Figure 3—figure supplement 2A**). Strains L1A, L2A and L5B displayed a tendency to induce more aggregates per field (median 42.5 [L1A], 40 [L2A] and 31.5 [L5B] vs. 22 [across all strains]) that were characterized by a less circular shape (i.e., higher aspect ratio) (median aspect ratios 1.38 [L1A], 1.35 [L2A] and 1.33 [L5B] vs. 1.25 [across all strains]) (**Figure 3—figure supplement 2B**). By contrast, L3 and L4 strains triggered the formation of markedly larger granulomas (median average area per granuloma in μm^2: 6,586.4 [L3] and 7,800 [L4] vs. 3,377.8 [L1], 5,199.2 [L2] and 4,638.4 [L5]) (**Figure 3—figure supplement 2C**). In order to simplify the ensuing analyses, we integrated these parameters into a granuloma score (see Methods section) that reflects the gamut of responses observed so that the bigger and more circular the granulomas, the higher the granuloma score (**Figure 3B**). Granuloma scores ranged from 42.2 to 1,801.1, with a median of 199.5. Infection with modern lineages, especially L3 and L4, led to granulomatous responses with significantly higher scores (median granuloma scores 205.6 [L2], 374.8 [L3] and 290.2 [L4] vs. 107.2 [L1] and 130.2 [L5]) (**Figure 3C**). Interestingly, the granuloma score showed a significant positive correlation with the respective strain growth rate (**Figure 3D**).

It has been reported that apoptosis of infected macrophages drives early dissemination and granuloma formation (Aguilo et al., 2013; Davis and Ramakrishnan, 2009). Therefore, we sought to evaluate macrophage apoptosis induced by the various strains in the context of granulomatous responses using flow cytometry (**Figure 4—figure supplement 1**). We did not observe significant differences in the total number of $CD11b^+$ macrophages recovered six days after infection with the various MTBC strains, nor in the percentage of necrotic macrophages (Annexin V^+ 7-AAD^+) (**Figure 4—figure supplement 2**). Overall, the percentage of apoptotic macrophages (Annexin V^+ 7-AAD^-) ranged from 24.3% to 65.2%, with a median of 41.2% (**Figure 4A**). Most of the strains shared intermediate levels of macrophage apoptosis, including the

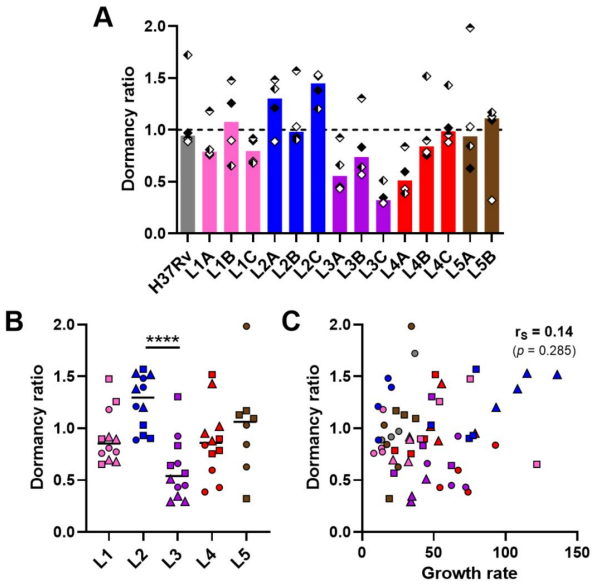

Figure 2.

Propensity to enter dormancy is particularly pronounced in lineage 2 and reduced in lineage 3 strains.

Bacilli recovered on day 8 post-infection were stained with Auramine-O (Au) and Nile red (NR) and quantified by fluorescence microscopy. Dormancy ratio was defined as the ratio between dormant (Au^- NR^+) and metabolically active (Au^+ NR^-) bacteria. Data stratified by **(A)** individual strain or **(B)** lineage. **(C)** Two-tailed Spearman's correlation analysis of dormancy ratio with growth rate. Colors indicate lineage and bars and horizontal lines represent medians. Shapes stand for (**A**) independent donors (n = 4) or (**B-C**) individual strains within the same lineage (LXA in circles, LXB in squares and LXC in triangles). Statistical analyses by (**A**) Friedman or (**B**) Kruskal-Wallis tests with *post hoc* Dunn's correction. ****, $p < 0.0001$.

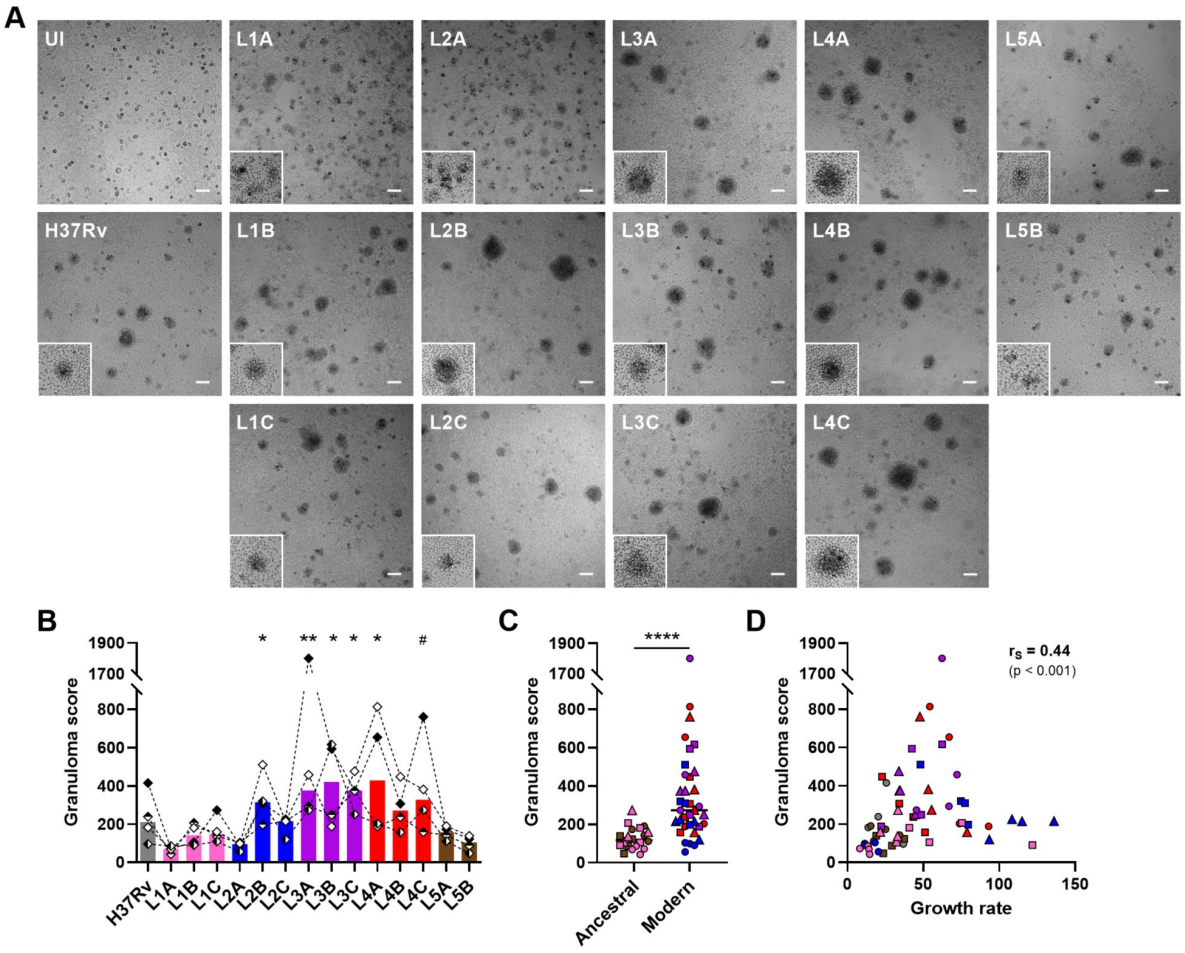

Figure 3.

MTBC strain diversity translates into a spectrum of granulomatous responses that correlates with bacterial growth.

(A) Bright field images of *in vitro* granulomas on day 7 post-infection from a representative donor. Scale bar = 100 μm. UI, uninfected. Lower left corner higher magnification inserts (200 μm sides) depict granulomas of characteristic size and morphology. **(B-D)** Number, area and aspect ratio of cell aggregates were quantified and integrated into a granuloma score (see Methods section). Granuloma scores stratified by **(B)** individual strain and **(C)** ancestral or modern lineage. **(D)** Two-tailed Spearman's correlation analysis of granuloma score with growth rate. Colors indicate lineage and bars represent medians. Shapes stand for (**B**) independent donors (n = 4), or (**C-D**) individual strains within the same lineage (LXA in circles, LXB in squares and LXC in triangles). Statistical analyses by (**B**) Friedman test with *post hoc* Dunn's correction (comparisons against L1A) or (**C**) two-tailed Mann-Whitney test. #, $p < 0.1$; *, $p < 0.05$; **, $p < 0.01$; ****, $p < 0.0001$.

reference strain H37Rv (median percentage of apoptotic macrophages 40.2%). By contrast, L1A and L2A strains, which were associated with the lowest growth rates and granulomatous responses, also exhibited a reduced induction of macrophage apoptosis (median percentages 29.6% and 30.2%, respectively); whilst L2C, the most virulent strain, induced the highest apoptosis levels (median percentage of apoptotic macrophages 49.4%). In fact, the percentage of apoptotic macrophages showed a significant positive correlation with the replication rate of the respective infecting MTBC strain (**Figure 4B**) as well as with granuloma scores (**Figure 4C**). Taken together, our results suggest that strains exhibiting greater proliferation are more prone to induce macrophage apoptosis and a stronger granulomatous response.

Rapid lymphocyte activation as well as CXCL9, granzyme B and TNF-α secretion are associated with reduced mycobacterial growth across the MTBC

We next sought to profile the immune granulomatous responses induced by the MTBC strains and relate them to their respective growth rate. We first monitored by flow cytometry lymphocyte proliferation using carboxyfluorescein succinimidyl ester (CFSE) dilution assay, as well as lymphocyte activation based on the expression of surface markers CD69, CD25, HLA-DR and CD38 on day six post-infection (**Figure 5—figure supplement 1**). We focused our analysis on CD69-, CD38-, CD25- and HLA-DR-expressing CD4 T cells, along with CD69- and CD38-expressing CD8 T cells, whose frequency increased consistently across all donors upon infection with at least one strain (compared to the uninfected control) (**Figure 5—figure supplement 2A-B**). Markedly stronger T cell responses were detected for one of the donors. This observation was consistent with a higher frequency of mycobacteria-specific CD4 T cells recalled by PPD stimulation (**Figure 5—figure supplement 2C**). To account for inter-donor variability, we scaled the responses of every donor dividing the individual response to each strain by the average response across all strains of that same donor (**Figure 5A**). As depicted in **Figure 5B**, granulomatous responses elicited by L1A, L2A and both L5 strains entailed marked CD4 T cell proliferation. Across all MTBC strains, proliferation was consistently associated with an increased expression of the assessed activation markers on both CD4 and CD8 T cells. Nevertheless, most activated CD4 T cells expressed only one of the studied markers (**Figure 5C**). Overall, ancestral lineages were the most potent inducers of all the aforementioned T cell populations (**Figure 5D** and **Figure 5—figure supplement 3A**), with CD38-expressing CD4 T cells constituting the most differentially induced population (median scaled frequencies 1.21 [ancestral] vs. 0.79 [modern]). Among modern lineages, L4 induced the strongest T cell activation (**Figure 5E** and **Figure 5—figure supplement 2B**), which actually was not statistically different from that elicited by ancestral strains (**Figure 5D** and **Figure 5—figure supplement 2A**). Infection with L4 strains resulted in significantly higher percentages of CD38-positive CD4 T cells compared to L2 Beijing strains (median scaled frequencies 0.94 vs. 0.54, respectively), while L3 strains elicited intermediate responses (median scaled frequency 0.73). When considering bacterial growth, strains eliciting an enhanced T cell response appeared among the ones replicating the least. We computed Spearman's rank correlation tests with Benjamin-Hochberg multiple testing correction between CD4 and CD8 T cell responses and the growth rate (**Figure 5F**). CD4 T cell proliferation as well as all expression of all activation markers exhibited significant, moderate to strong, negative correlations with MTBC strain growth rate, with the expression of CD38 resulting in the strongest coefficient. Activation of CD8 T cells, determined by the expression of either CD38 or CD69, was also significantly associated with a hampered mycobacterial proliferation. Shedding light on what distinguishes granulomas that are protective from those that support bacterial growth, a significant negative correlation between macrophage apoptosis induction and T cell activation can be observed specifically with activated CD4 T cells expressing CD38 ($r_S = -0.36$, $p < 0.05$) or CD69 ($r_S = -0.40$, $p < 0.01$). Taken together, our data indicate that stronger T cell activation is associated with MTBC isolates exhibiting low bacterial replication, irrespective of the lineage they belong to.

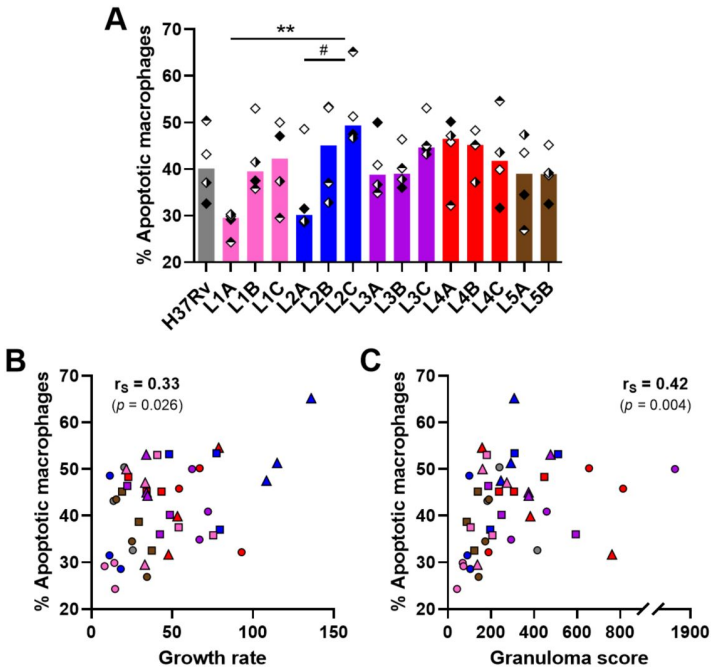

Figure 4.

Macrophage apoptosis is positively associated with mycobacterial growth rate and granuloma score.

(A) Percentage of apoptotic macrophages (CD11b$^+$ Annexin V$^+$ 7-AAD$^-$) on day 6 post-infection quantified by flow cytometry. **(B-C)** Two-tailed Spearman's correlation analysis of macrophage apoptosis with (**B**) growth rate or (**C**) granuloma score. Colors indicate lineage and bars represent medians. Shapes stand for (**A**) independent donors (n = 4) or (**B-C**) individual strains within the same lineage (LXA in circles, LXB in squares and LXC in triangles). (**A**) Statistical analysis by Friedman test with *post hoc* Dunn's correction. #, $p < 0.1$; **, $p < 0.01$.

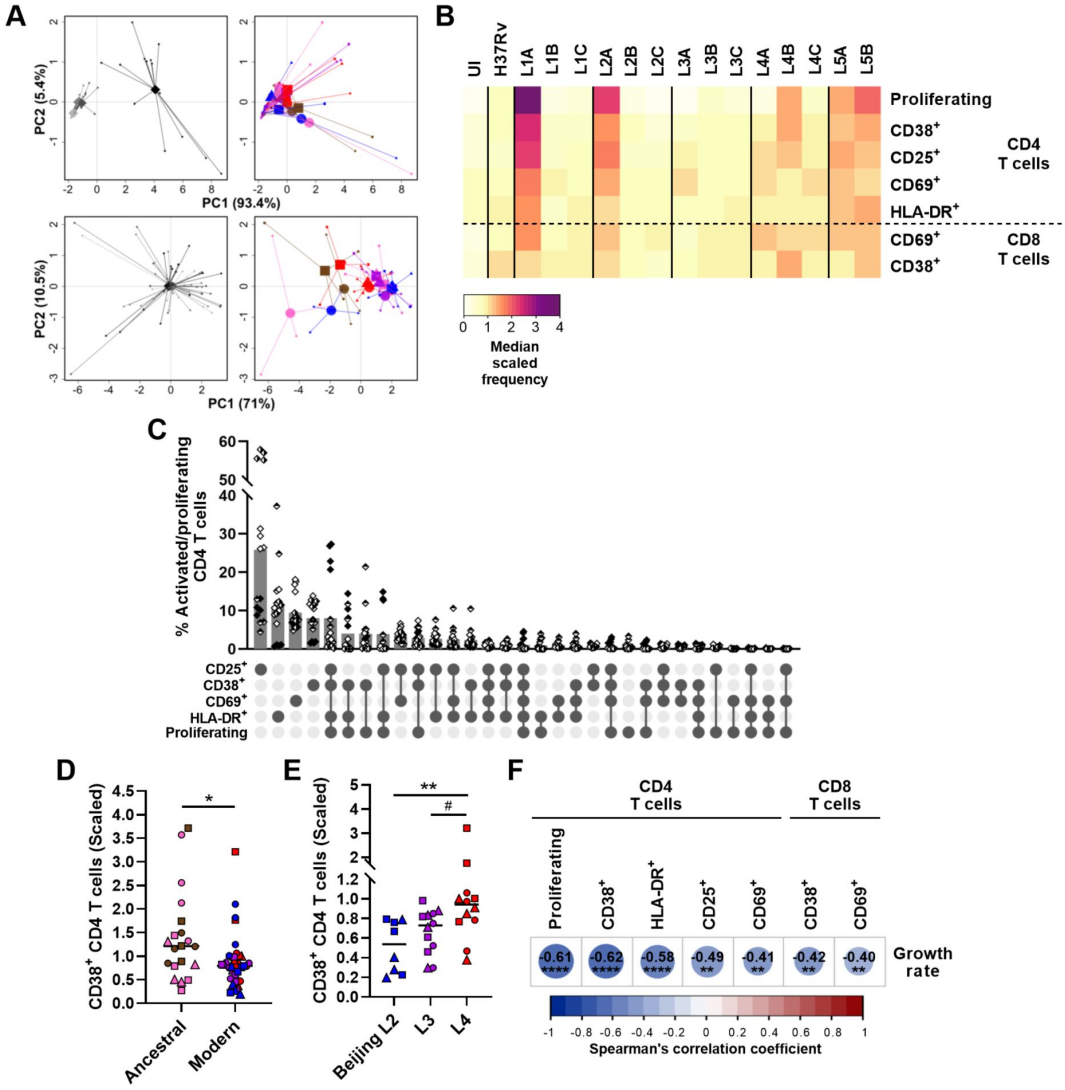

Figure 5.

Activation and proliferation of T cells is associated with reduced mycobacterial growth across the MTBC.

Percentage of activated (expressing any of the markers) and proliferating (CFSE^{-}) T cells on day 6 post-infection was quantified by flow cytometry. **(A)** Principal component (PC) analysis using raw (top panels) or scaled (lower panels) data. Data were grouped by donor (left panels), with grey shades representing independent donors (n = 4); or by MTBC infecting strain (right panels), with colors indicating lineage and shapes standing for individual strains within the same lineage (LXA in circles, LXB in squares and LXC in triangles). **(B)** Heatmap representing the median scaled frequencies induced by each MTBC strain. UI, uninfected. **(C)** Marker co-expression on the activated/proliferating CD4 T cells induced by L1A, L2A and L5 strains. Bars represent the mean percentage of cells expressing the indicated marker combination and each filling pattern of the shapes corresponds to an individual donor. **(D-E)** Percentage of CD38^{+} CD4 T cells elicited by (**D**) ancestral or modern lineages, or (**E**) specific modern lineages. Colors and shapes same as in (**A**) and horizontal lines represent medians. Statistical analyses by (**D**) two-tailed Mann-Whitney or (**E**) Kruskal-Wallis tests with *post hoc* Dunn's correction. **(F)** Heatmap of Spearman's correlation coefficients of activated/proliferating T cell populations with MTBC growth rate (two-tailed, *post hoc* Benjamini-Hochberg corrected). # $p < 0.1$; *, $p < 0.05$; **, $p < 0.01$; ****, $p < 0.0001$.

Subsequently, we investigated whether a panel of soluble immune factors —linked or not to T cell activation— may also be associated with a reduced bacterial growth. We focused our analysis on molecules present in granuloma supernatants on days one or eight post-infection that were modulated by the infection (**Figure 6—figure supplement 1**). We again scaled the data to account for inter-donor variability, as described above (**Figure 6A**). Differentially modulated molecules included the innate cytokines TNF-α and IL-1β at both time points, IL-10 and the chemokine CXCL9 at the earlier time point, and IFN-ψ, IL-17 (A and F), IL-22, IL-13 and granzyme B at the later (**Figure 6B**). Among these, IL-1β and IL-13 displayed significant lineage-associated trends. L4, and to a lesser extent L3, induced a significantly higher secretion of IL-1β on day one post-infection (median scaled responses 1.54 [L4] and 1.31 [L3] vs. 0.55 [L1], 0.94 [L2], and 0.89 [L5]) (**Figure 6C**, *left*). This pattern remained at the later time point for L4 (median scaled responses 1.37 [L4] vs. 0.79 [L1], 0.95 [L2], 1.17 [L3] and 1.03 [L5]) (**Fig 6B**, *right*). Interestingly, the IL-1β response on day one post-infection showed a moderate positive correlation with granuloma score (**Figure 6D**). In order to investigate the influence of IL-1β levels on the granulomatous response, IL-1β was blocked throughout the infection using gevokizumab (Issafras et al., 2014) and granuloma formation was monitored on day seven post-infection (**Figure 6E**). Neutralization significantly decreased the score of granulomas generated by high IL-1β inducer strain L4C, whereas it had no effect on granulomas associated with low IL-1β inducer strain L1A, thereby establishing a cause-effect relationship between these two phenotypes. Moreover, we found that the CD4 T helper 2 cytokine IL-13 was preferentially induced in the context of infection with modern lineages compared to ancestral lineages (median scaled responses 1.18 [modern] vs. 0.78 [ancestral]) (**Figure 6F**). While we found no significant correlation for IFN-ψ, induction of CXCL9 secretion on day one post-infection, and granzyme B as well as TNF-α on day eight post-infection were associated with a reduced MTBC bacterial proliferation (**Figure 6G**). However, blocking of CXCL9 during the infection failed to confirm causality since it did not impact bacterial load of either the high CXCL9 inducer strain L1A or the low CXCL9 inducer strain L2C (**Figure 6H**). Altogether, these results convey that a robust T cell activation characterized by an early CXCL9 detection and higher levels of TNF-α and granzyme B may orchestrate the control of mycobacterial growth.

Discussion

There is increasing epidemiological and experimental evidence that MTBC strain diversity may influence pathogenicity. Yet, only a small number of studies based on human specimens have compared a diverse range of strains belonging to more than two lineages (Portevin et al., 2011; Reiling et al., 2013). Here, we combine an *in vitro* granuloma model (Arbues et al., 2020a; Arbues et al., 2021) with a set of representative L1 to L5 strains (Borrell et al., 2019) to demonstrate that MTBC genetic variation affects the crosstalk with human immune cells. The model encompasses all PBMC-derived cell types involved in TB immune responses, but lacks granulocytes (i.e. neutrophils, eosinophils, basophils and mast cells). Consequently, the interface between the MTBC strains and neutrophils —which play a pathogenic role in TB by providing a permissive environment for mycobacterial replication (Andrews et al., 2024; Gideon et al., 2019; Lowe et al., 2013)— could not be investigated. We show that MTBC isolates display a range of growth rates correlating with the induction of macrophage apoptosis and the extent of the resulting granulomatous structures. This result is in agreement with the current view of the tuberculous granuloma as a structure that, beyond functioning as purely host-protective, is exploited by pathogenic mycobacteria as a niche for proliferation and dissemination (Pagan and Ramakrishnan, 2014). Our data reveal various features that associate with certain MTBC lineages and/or strains. Noteworthy, we have identified immune response traits that correlate with hampered mycobacterial proliferation.

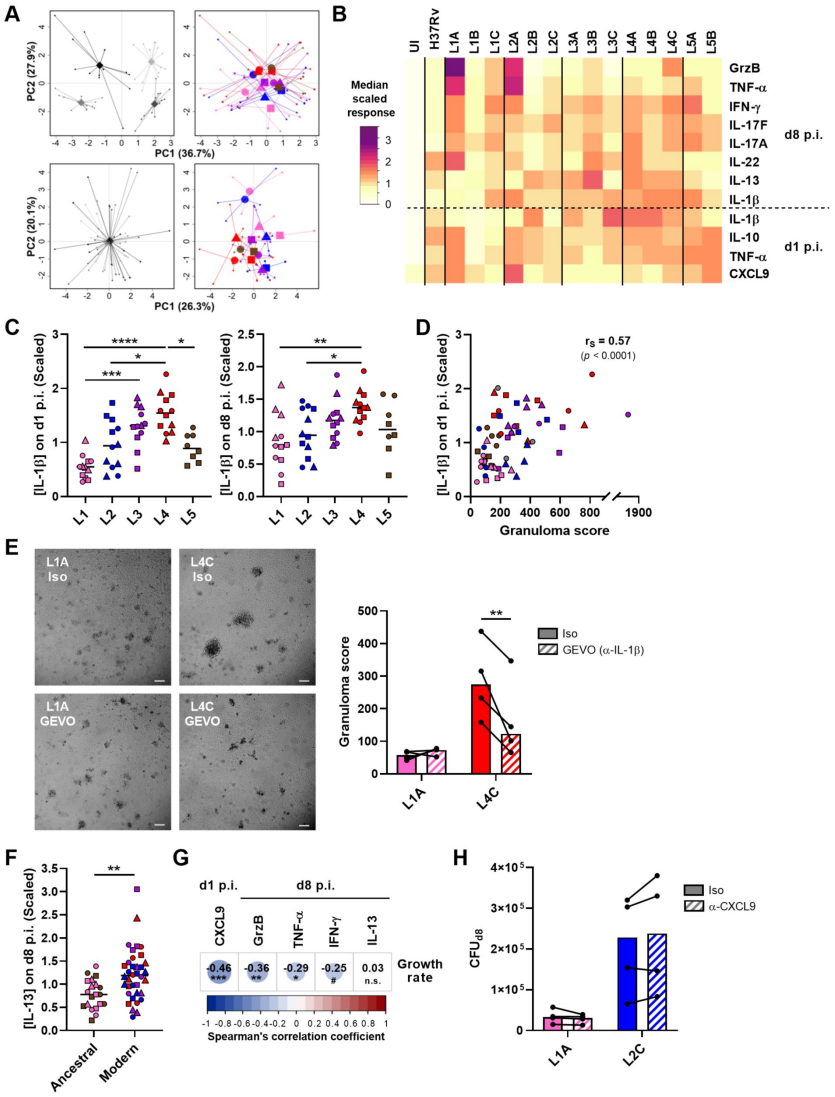

Figure 6.

CXCL9, granzyme B and TNF-α secretion is associated with reduced mycobacterial growth across the MTBC.

The concentration of soluble mediators in the supernantant of *in vitro* granulomas on days 1 and 8 post-infection (p.i.) was quantified by multiplex bead-based immunoassay. **(A)** Principal component (PC) analysis was performed using raw (top panels) or scaled (lower panels) concentrations. Data were grouped by donor (left panels), with grey shades representing independent donors (n = 4); or by MTBC infecting strain (right panels), with colors indicating lineage and shapes standing for individual strains within the same lineage (LXA in circles, LXB in squares and LXC in triangles). **(B)** Heatmap of the median scaled response induced by each MTBC strain. UI, uninfected; GrzB, granzyme B. **(C)** IL-1β response stratified by lineage. Colors and shapes same as in (**A**) and horizontal lines represent medians. **(D)** Two-tailed Spearman's correlation analysis of IL-1β response on day 1 p.i. with granuloma score. Colors and shapes same as in (**A**). **(E)** Effect of early blocking of IL-1β on granuloma formation using gevokizumab (GEVO). Bright field images of *in vitro* granulomas on day 7 p.i. from a representative donor. Iso, isotype control. Scale bar = 100 µm. Granuloma score was calculated as indicated in **Figure 3**. Colors indicate lineage, bars represent medians, and data from the same donor are connected through lines. **(F)** IL-13 response stratified by ancestral or modern lineages. Colors and shapes same as in (**A**) and horizontal lines represent medians. **(G)** Heatmap representing Spearman's correlation coefficients of cytokine concentrations with MTBC replication rate (two-tailed, *post hoc* Benjamini-Hochberg corrected). **(H)** Effect of early blocking of CXCL9 on bacterial load on day 8 p.i. Colors indicate lineage, bars represent medians, and data from the same donor are connected through lines. Statistical analyses by (**C**) Kruskal-Wallis test with *post hoc* Dunn's correction, (**E, H**) two-way ANOVA with *post hoc* Sidak's correction, or (**F**) two-tailed Mann-Whitney tests. n.s., $p > 0.1$; #, $p < 0.1$; *, $p < 0.05$; **, $p < 0.01$; ***, $p < 0.001$; ****, $p < 0.0001$.

"Modern" lineages (L2 to L4) are often associated with globally spread TB epidemics, whereas TbD1-intact "ancestral" lineages (L1 and L5 to L10) rather represent endemic strains restricted to a given geographical area. A general consensus arose that strains belonging to modern lineages would exhibit enhanced capacities to proliferate compared to those from ancestral ones (Reiling et al., 2013; Romagnoli et al., 2018). Actually, in an elegant work using recombinant strains, Bottai and colleagues demonstrated that TbD1 deletion significantly increases MTB virulence in relevant infection models (Bottai et al., 2020). In line with these previous studies, ancestral lineages display reduced virulence in *in vitro* granulomas compared to the modern lineages. L1 is found in countries along the rim of the Indian Ocean. This geographical confinement together with experimental evidence (Bottai et al., 2020; Reiling et al., 2013; Romagnoli et al., 2018) prompted a general view of L1 as a low virulence lineage. Our data showed that, overall, L1 exhibited lower virulence than modern lineages. Nonetheless, we observed a significant intra-lineage variation, with strain L1C exhibiting a growth rate comparable to those of strains belonging to modern lineages. This phenotypic variability may be a reflection of the highly diverse population structure exhibited by this lineage (Netikul et al., 2021). In line with our findings, Mitchison and colleagues also documented a wide range of virulence among South Indian isolates, with one-third of them being as virulent as the British ones (Mitchison et al., 1960). Even though it is unclear whether all those strains belonged to L1, we can assume that a majority of them were when considering epidemiological data (Poonawala et al., 2020). These results exposing virulence variation across L1 isolates challenge the "low virulence" attribute generally given to L1. However, a recent report revealed that the contribution of L1 to the global TB pandemic is generally undervalued (Netikul et al., 2021). Due to its prevalence in countries with the highest TB incidence, L1 was estimated to account for 28% of the total TB cases. Interestingly, the strains with the higher replication rates, L1B and L1C, were isolated from patients of Indian and Filipino origin and belong to the most common sublineages, L1.1.2 and L1.2.1, respectively. Taken together these data suggest that some L1 sublineages may have evolved mechanisms to compensate for the attenuation associated to the presence of TbD1 (Bottai et al., 2020). Meanwhile, L5, previously known as *M. africanum* 1, is geographically restricted to West Africa. Experimental data on L5 are scarce and most of our understanding about TB caused by *M. africanum* derives from the study of L6, previously reported as *M. africanum* 2 (Silva et al., 2022). In contrast to the down-regulation of the DosR regulon reported in the sputum of L6-infected patients compared to L4 (Ofori-Anyinam et al., 2017), we observed a similar induction of dormant-like mycobacteria in L4 and L5. In accordance with their ancestral genotype, both L5 strains displayed comparable low replication rates and elicited increased frequencies of activated T cells. Nevertheless, we cannot dismiss a potential contribution of host genetics to the apparent attenuation of L5. In Ghana, infection by L5 has been associated with the Ewe ethnic group (Asante-Poku et al., 2015). L5 strains displayed lower growth in macrophages from the Akan ethnic group; still, proliferation in Ewe's macrophages was comparable to that of L4 isolates (Osei-Wusu et al., 2023).

The three modern lineages (L2 to L4) displayed comparable growth rates overall. Again, substantial strain-to-strain variability was observed within L2. The L2 Proto-Beijing strain L2A was markedly attenuated to a level comparable to that of the ancestral lineages. At the other end of the virulence spectrum, the representative of the most recently evolved L2 strains, the so-called "modern" L2 Beijing, displayed the highest proliferative capacity across all the MTBC strains studied. For its part, the "ancestral" Beijing isolate exhibited a bacterial burden comparable to those of strains belonging to other modern lineages. This finding suggests that L2 strains have evolved towards increased virulence. This is also consistent with prior studies showing that modern Beijing strains exhibited enhanced virulence in mice compared to those with an ancestral genotype (Ribeiro et al., 2014). The L2 Beijing sublineage has received particular attention due to its high transmissibility and virulence in cellular and animal models (Guerra-Assuncao et al., 2015; Manca et al., 2001; Tram et al., 2018; Tsenova et al., 2005). One previously identified mechanism contributing to the hyper-virulent phenotype of L2 Beijing strains is the inhibition of the production of pro-inflammatory cytokines (Reed et al., 2004; Wang et al., 2010). Likewise, we found that both L2 Beijing strains were poor inducers of T cell activation

and pro-inflammatory cytokines. By contrast, we found the high replication rate of L4 strains to be accompanied by a significant T cell activation and high levels of IFN-ψ. These data are consistent with the fact that MTBC strain CDC1551, responsible for one of the most studied L4 outbreaks, was characterized by very large skin test responses in infected subjects and a robust pro-inflammatory immune response in mice and in human monocytes (Manca et al., 1999). In addition, we observed that L4, and to a lesser extent L3, promoted an increased secretion of IL-1β. Romagnoli and collaborators showed that higher IL-1β levels trigger autophagy; however, L4 isolates evade subsequent lysosomal degradation (Romagnoli et al., 2018). Despite its protective role (Mayer-Barber et al., 2010), increased IL-1β levels in the bronchoalveolar lavage or serum of TB patients have been associated with presence of cavities and higher bacterial loads in sputum (Sigal et al., 2017; Tsao et al., 2000). Consonantly, high transmission strains induced an increased expression of IL-1β in the lungs of infected mice compared to low transmission ones (Lovey et al., 2022). Therefore, our and others' findings indicate that L4 constitutes an example of impeded pro-inflammatory responses not to be the only way for the MTBC members to achieve global success.

Lastly, L3 was characterized by a tendency to preferentially remain in a metabolically active state, in contrast with the increased propensity of L2 to enter dormancy, which was previously reported under standard culture conditions in broth (Reed et al., 2007). Whilst it was originally thought that this phenotype could be responsible for the increased virulence displayed by L2 Beijing strain in the mouse model, subsequent studies disproved this hypothesis (Domenech et al., 2017). In line with this, our results show that even in the context of hypoxic granulomatous responses – which are lacking in the mouse model– there was no correlation between the propensity to switch into a dormant state and virulence, as reflected in bacterial burden in our model, across MTBC lineages. Last but not least, we have identified immune response traits that correlate with the hampered mycobacterial proliferation exhibited by various MTBC strains of independent lineages. T cells are essential for immunity against the MTBC (Kaufmann, 2002); hence, it is unsurprising that the level of CD4 and CD8 T cell activation inversely correlated with mycobacterial growth rate. Increased levels of CXCL9, granzyme B and TNF-α were also found to be associated with a better control of MTBC proliferation. Among the identified soluble factors, the prominent protective role of TNF-α in TB is well-known (Flynn et al., 1995). CXCL9's paradigmatic function is directing the migration of CXCR3-expressing cells (i.e., T helper 1 CD4 T cells, effector CD8 T cells and natural killer cells) (Groom and Luster, 2011). CXCL9 has attracted attention as potential biomarker for TB diagnosis and treatment monitoring (Ambreen et al., 2021; Uzorka et al., 2022). A blocking experiment failed to establish a direct relationship between CXCL9 levels and MTBC growth. Warranting further investigations, we hypothesize that chemokines such as CXCL10 and CXCL11 that were not included in our screening panel and that are also signaling through CXCR3 may be acting in concert with CXCL9 to drive this phenomenon. Indeed, some evidence suggests that CXCR3 ligands play a role in the positioning of effector cells within the lung for control of MTB proliferation. Protective vaccination in mice triggered the production of chemokines, including CXCL9, in the lung and associated recruitment of $CXCR3^+$ CD4 T cells (Khader et al., 2007). In addition, increased densities of $CXCR3^+$ CD4 T cells were found in the lungs of latently infected non-human primates (NHPs) relative to those with active TB (Shanmugasundaram et al., 2020). CXCL9 has also been reported as a new marker of trained immunity in mycobacterial growth inhibition assays (Joosten et al., 2018). Recently MTBC-exposed individuals, which exhibited the strongest control of mycobacterial proliferation, produced increased levels of CXCL9. Notably, our findings are in line with recent reports highlighting an important role of granzyme B in the control of MTBC infection in the early stages of TB. In NHPs, low burden granulomas were associated with a higher proportion of a T/NK cell cluster expressing granzyme B (Gideon et al., 2022). Furthermore, individuals with latent TB infection exhibited increased expression of granzyme B in activated NK cells (Esaulova et al., 2021). IFN-ψ levels did not exhibit a significant correlation, only a trend, with mycobacterial replication rate in *in vitro* granulomas. Our finding is supported by TB vaccine trials demonstrating that induction of strong IFN-ψ responses does not translate into enhanced

protection (Tameris et al., 2013). However, strains with low replication rates were among those inducing high IFN-ψ levels. These results therefore suggest that IFN-ψ is required, yet not sufficient to mediate protection.

In summary, our investigation exposed various features that associate with certain MTBC lineages and/or strains, thereby reinforcing the concept that effective treatments and vaccines need to be tailored. We advocate *in vitro* granuloma models as relevant tools to understand the implications of MTBC strain diversity on the interaction with humans of diverse genetic backgrounds and to assess protective traits elicited by vaccines.

Materials and methods

Isolation of human peripheral blood mononuclear cells (PBMCs)

Buffy coats from healthy, anonymous blood donors (under informed consent) were purchased from the Interregionale Blutspende SRK AG (Bern, Switzerland). PBMCs were isolated from buffy coats by Ficoll-Paque (GE Healthcare) density-gradient and washed twice with RPMI-1640 with L-glutamine (RPMI; Sigma-Aldrich). Aliquots were cryopreserved in RPMI supplemented with 10% DMSO (Sigma-Aldrich) and 40% fetal bovine serum (FBS; Gibco) and stored in liquid nitrogen. Isolated PBMCs were systematically tested for CD4 T cell reactivity against PPD (purified protein derivative; Statens Serum Institute, RT23) as previously reported by our laboratory (Arbues et al., 2020a). Prior to use, PBMCs from PPD-reactive donors were thawed, washed twice in RPMI containing 10% FBS (RPMI-FBS) and benzonase (12.5 U/ml; BioVision) and rested in RPMI-FBS overnight at 37°C-5% CO_2. Trypan blue dye exclusion method was used to confirm sample viability of above 95%. PBMC concentration was adjusted to 10^7 cells/ml in RPMI supplemented with 20% human AB serum (PAN-Biotech) (RPMI-HS).

Culture and preparation of disperse suspensions of *M. tuberculosis* complex (MTBC) strains

We selected 14 isolates (**Table 1**) from a reference set of clinical strains covering much of the global diversity of the human-adapted MTBC (Borrell et al., 2019). This strain collection comprises drug-susceptible strains isolated from patients of diverse origin that can be successfully grown in culture. The strain subset used encompasses three strains per lineage for L1 to L4 and two L5 strains. The laboratory strain H37Rv, which was used for the implementation of the model (Arbues et al., 2020a), was included as a reference. We excluded L6 from the present study due to its characteristic significantly slower growth in axenic culture (Gehre et al., 2013). L7 to L9 were not included since they have only been described recently and the number of available isolates is very scarce.

MTBC strains were cultured under gentle agitation in Middlebrook 7H9 broth supplemented with 10% ADC (5% bovine albumin fraction V, 2% dextrose and 0.003% catalase), 0.5% glycerol (PanReac AppliChem) and 0.05% Tween-80 (Sigma-Aldrich), additionally enriched with 40 mM sodium pyruvate (Sigma-Aldrich) for L5 strains. Upon reaching mid-exponential phase (OD_{600} between 0.4 and 0.8), bacteria were washed with PBS containing 0.1% Tween-80 (PBST) and resuspended in RPMI-FBS. The resultant mycobacterial suspension was dispersed by water-bath sonication (XUB5, Grant Instruments) for 2 min, and then centrifuged at 260 ×*g* for 5 min. The upper part of the supernatant was recovered and cryopreserved by adding 5% glycerol (final) and stored at –80°C. Concentration of the frozen stocks was quantified by colony forming unit (CFU) assessment (see below).

Generation and quantification of three-dimensional (3D) *in vitro* granulomas

PBMCs from four healthy blood donors were infected independently with the selected MTBC isolates, and subsequently embedded within an extracellular matrix (ECM) composed of collagen and fibronectin, the main components of the lung extracellular matrix, as previously reported (Arbues et al., 2020b). Briefly, an ECM solution composed of 950 µl/ml of collagen (PureCol, 3 mg/ml; Advanced BioMatrix), 50 µl/ml of PBS 10X, 4 µl/ml of human fibronectin (1 mg/ml; Sigma-Aldrich), and 10 µl of 1 N NaOH (Sigma-Aldrich) was prepared and incubated at 4°C for 90 min. Rested PBMCs were infected with the various MTBC strains at a multiplicity of infection (MOI) of 1:200 (bacteria:PBMCs), or left uninfected when required. Thereafter, 1.25×10^6 PBMCs per well were distributed across 48-well plates and mixed with the pre-incubated ECM in a 1:1 (v/v) ratio. The ECM was left to set for 45 min at 37°C-5% CO_2 before 250 µl of RPMI-HS were added.

Granuloma formation was monitored on day 7 post-infection using a Leica THUNDER Imager Live Cell (Leica). Cellular aggregates present in a representative bright field per donor and condition were enumerated and measured using ImageJ 1.52n (National Institutes of Health, US). The total number of granulomas, their size and aspect ratio (i.e., the ratio of the major axis to the minor axis; and so, and aspect ratio of 1 corresponds to a circle, and >1 to an ellipse) were integrated into a granuloma score as follows: the area of each individual granuloma was divided by its corresponding aspect ratio, then the average was calculated and divided by the total number of aggregates.

$$Granuloma\ score\ = \frac{\overline{X}\ (granuloma\ area/aspect\ ratio)}{No.\ aggregates}$$

Thus, the induction of numerous but small aggregates with an elongated shape translates into the lowest granuloma scores; whilst generation of bigger, even if fewer, circular aggregates results in higher values.

Retrieval of mycobacteria

At the relevant time points, supernatant was removed and the ECM was digested with 125 µl of collagenase (1 mg/ml; Sigma-Aldrich) for 40 min at 37°C-5% CO2. Subsequently, host cells were lysed by adding 125 µl of 0.4% Triton X-100 (Sigma-Aldrich) and incubating for 20 min at room temperature. Released bacilli were subsequently used for bacterial load quantification by CFU assessment and dual auramine-O/Nile red staining.

CFU assessment

Briefly, 10-fold serial dilutions of the mycobacterial suspensions were prepared in triplicate in PBST and plated on 7H11 agar (BBL) plates supplemented with 0.5% glycerol and 10% OADC (0.05% oleic acid in ADC), additionally enriched with 40 mM sodium pyruvate for L5 strains. Plates were incubated at 37°C-5% CO_2 for 3-4 weeks.

Dual Auramine-O/Nile red staining

Bacilli retrieved on day 7 post-infection were inactivated with 1X CellFIX (BD) for 20 min at room temperature and afterwards stored at 4°C until processing. Fixed samples were centrifuged at 10,000 ×*g* for 5 min to remove the fixative prior being resuspended in water. Subsequently they were spotted on glass slides, air dried and heat fixed at 70°C. Fluorescent acid-fast staining using TB Fluorescent Stain Kit M (BD) was performed in combination with neutral-lipid staining dye Nile red (Sigma) (Arbues et al., 2020a). Briefly, each sample was stained with Auramine-O for 20 min, decolorized for 30 s, covered with Nile red (10 µg/ml) for 15 min and counterstained with potassium permanganate for 2 min, including gentle washes with distilled water between each

step. Air-dried, stained slides were mounted using Vectashield mounting medium (Vectorlabs) and examined using a Leica DM5000 B fluorescence microscope (Leica). For quantification purposes, at least 200 bacteria per sample were counted manually.

Macrophage cell death quantification

On day 6 post-infection, cells were released from the ECM by collagenase digestion as described above. Subsequently, they were pelleted at 400 ×*g* for 5 min and extracellularly stained as follows. Cells were incubated for 15 min at room temperature in 100 µl of Annexin binding buffer (ABB, BioLegend) containing APC-labeled Annexin V, 7-AAD, and fluorochrome-labeled antibodies (BioLegend) against human CD3 (Pacific blue, clone UCHT1), CD19 (BV510, clone HIB19), and CD11b (PE-Cy7, clone ICRF44). Samples were washed once with ABB and fixed in 1X CellFIX (BD) for 20 min at room temperature. Samples were acquired on a MACSQuant Analyzer 10 (Miltenyi Biotec) and processed using FlowJo 10.6.1 (BD).

Assessment of lymphocyte activation and proliferation

Prior to infection for the generation of 3D *in vitro* granulomas, rested PBMCs were labeled with carboxyfluorescein succinimidyl ester (CFSE). Briefly, PBMCs were resuspended in PBS containing 1 µM CFSE (BioLegend) at 5×10^6 cells/ml and incubated at 37°C-5% CO_2 for 10 min. After quenching the staining by adding 2.5 volumes of PBS containing 20% FBS, cells were pelleted and resuspended at 10^7 cells/ml in RPMI-HS.

On day 6 post-infection, cells were released from the ECM by collagenase digestion as described above. Subsequently, they were pelleted at 400 ×*g* for 5 min and extracellularly stained following a standard protocol. Cells were incubated for 20 min at room temperature in 100 µl of FACS buffer (0.1% FBS in PBS) containing fluorochrome-labeled antibodies (BioLegend) against human CD3 (Pacific blue, clone UCHT1), CD4 (PE-Cy7, clone RPA-T4), CD8 (BV510, clone HIT8a), CD19 (BV510, clone HIB19), CD25 (PE, clone BC96), CD69 (PerCP, clone FN50), CD38 (APC, clone HIT2), and HLA-DR (APC-Cy7, clone L243). Samples were washed once with FACS buffer and fixed in fixation buffer (BioLegend) for 20 min at room temperature. Samples were acquired on a MACSQuant Analyzer 10 (Miltenyi Biotec) and processed using FlowJo 10.6.1 (BD).

Quantification of soluble factors

Supernatants collected on day 1 and 8 post-infection, and stored at –80°C in the meantime, were filter-sterilized no more than 24 h prior to analysis by multiplex bead-based immunoassay. A ProcartaPlex custom panel (including CCL2/MCP-1, CCL3/MIP-1α, CXCL9/MIG, TNF-α, IL-1β, IL-2, IL-6, IL-10, IL-12p70, IL-13, IFN-α, IFN-ψ, GM-CSF, granzyme B and MMP-1) (Invitrogen) and the Bio-Plex Pro™ human Th17 cytokine panel (Bio-Rad) (including IL-17A, IL-17F, IL-21, IL-22 and IL-23) were used according to the manufacturer's recommendations and acquired on a Luminex Bio-Plex 200 platform and Bio-Plex Manager 6.0 software (Bio-Rad). Culture medium was measured in parallel to the samples to assess any potential residual presence of the target biomolecules in the human serum. Results were analyzed using R package nCal (Fong et al., 2013).

Blocking of IL-1β and CXCL9 early responses

In order to evaluate the impact of blocking IL-1β response on granuloma formation, PBMCs were treated on infection day with 200 ng/ml of anti-IL-1β biologic gevokizumab (Ichorbio) or a human IgG2 isotype control (BioLegend, clone QA16A13). On day 4 post-infection, supernatant was removed and replenished with fresh, antibody-containing RPMI-HS. Granuloma formation was monitored on day 7 post-infection and granuloma score calculated as described in the Generation and quantification of three-dimensional (3D) *in vitro* granulomas section.

Similarly, to assess the effect of blocking CXCL9 on bacterial proliferation, PBMCs were treated on infection day with 200 ng/ml of a neutralizing antibody (BioLegend, clone A16023A) or a mouse IgG1 isotype control (BioLegend, clone MG1-45). On day 4 post-infection, supernatant was removed and replenished with fresh, antibody-containing RPMI-HS. Bacterial load was quantified on day 8 post-infection as described in the Retrieval of bacteria and CFU assessment sections.

Quantification and statistical analysis

GraphPad Prism 8.2.1 and R.4.3.1 and R studio 2023.06.1-524 were used to produce quantitative graphical representations of the generated data and to perform statistical analyses. The nature of the tests and definition of center and significance levels is specified within the respective figure legend.

Additional information

Funding

This work was supported by the Swiss National Science Foundation (SNSF197838).

Author contributions

Conceptualization, A.A. and D.P.; Methodology, A.A., S.S., and D.P.; Investigation, A.A., S.S., and M.R.; Formal analysis, Visualization, A.A, S.S. and D.P.; Writing – Original Draft, A.A, S.S. and D.P.; Writing – Review & Editing, A.A., S.S., S.B., S.G. and D.P.; Funding Acquisition, D.P.; and Supervision, D.P. The authors declare no competing interests.

Figure 1—figure supplement 1.

Bacterial load of the selected MTBC isolates in human *in vitro* granulomas.

Colony forming units (CFU) were quantified on **(A)** day 1 and **(B)** day 8 post-infection. Colors indicate lineage, bars represent medians and shapes stand for independent donors (n = 4). Statistical analysis by Friedman test with *post hoc* Dunn's correction. #, $p < 0.1$; **, $p < 0.01$; ***, $p < 0.001$.

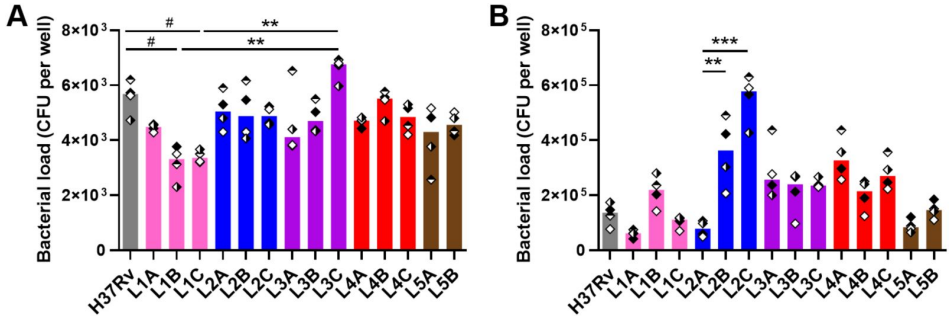

Figure 2—figure supplement 1.

Auramine-O/Nile red profile of the selected MTBC isolates.

Bacilli recovered on day 8 post-infection were stained with Auramine-O (Au) and Nile red (NR) and quantified by fluorescence microscopy. **(A)** Photomicrograph picturing representative staining phenotypes. Scale bar = 10 µm. Data stratified by **(B)** individual strain or **(C)** lineage. Bars represent medians and shapes stand for (**B**) independent donors (n = 4) or (**C**) individual strains within the same lineage (LXA in circles, LXB in squares and LXC in triangles).

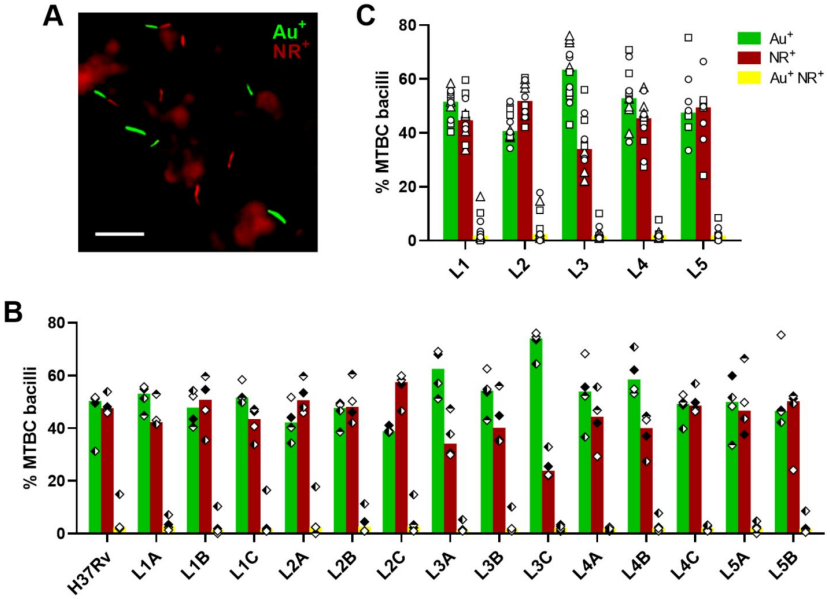

Figure 3—figure supplement 1.

Granulomatous response variability across MTBC strains is consistent across independent donors.

Bright field images of *in vitro* granulomas on day 7 post-infection from MTBC strains representative of the spectrum of granulomatous responses observed. Scale bar = 100 µm.

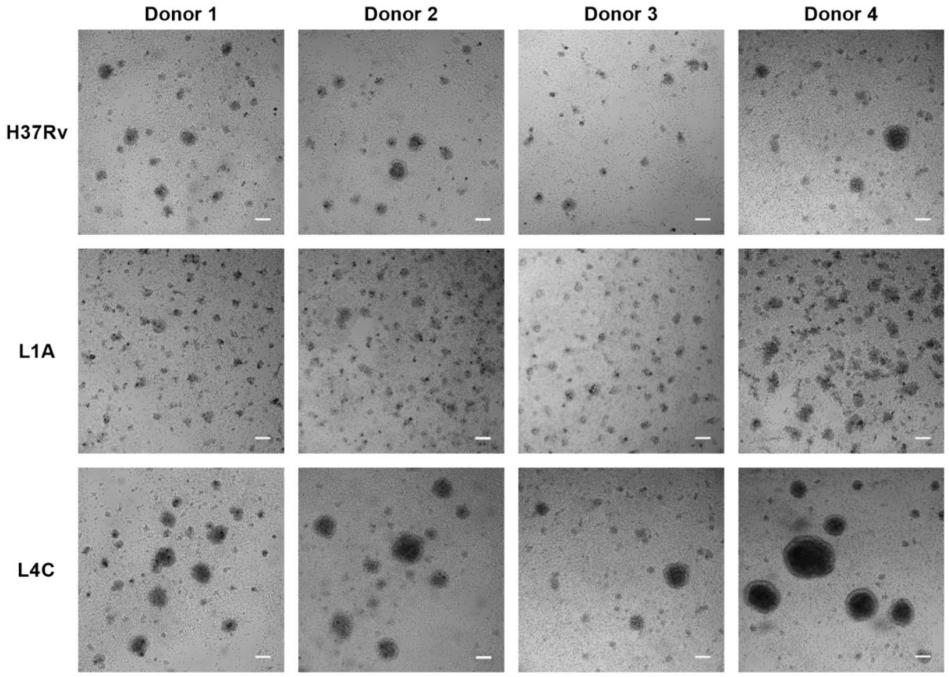

Figure 3—figure supplement 2.

The number, shape and size of *in vitro* granulomas vary depending on the MTBC infecting strain.

(A) Total number (no.) of granulomas, as well as their individual **(B)** aspect ratio and **(C)** area were quantified on a representative bright field for each strain and donor. Colors indicate lineage, shapes correspond to individual donors (n = 4) and bars represent medians. Statistical analysis by Friedman test with *post hoc* Dunn's correction (comparisons against H37Rv). #, $p < 0.1$; *, $p < 0.05$; **, $p < 0.01$.

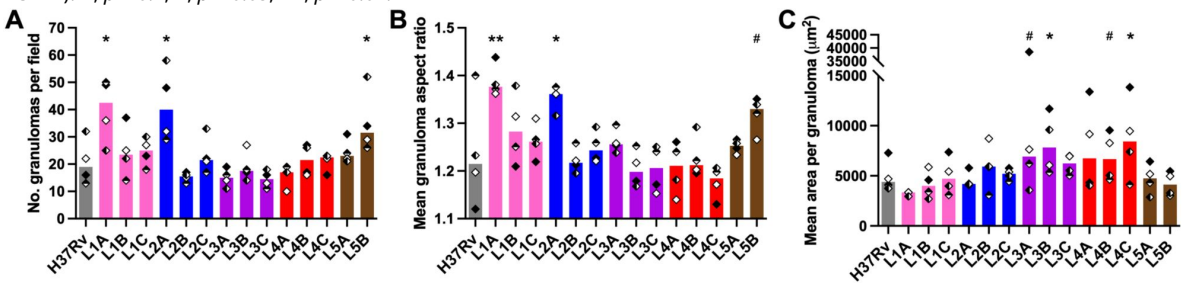

Figure 4—figure supplement 1.

Flow cytometry gating strategy for the quantification of cell death induction in CD11b$^+$ macrophages.

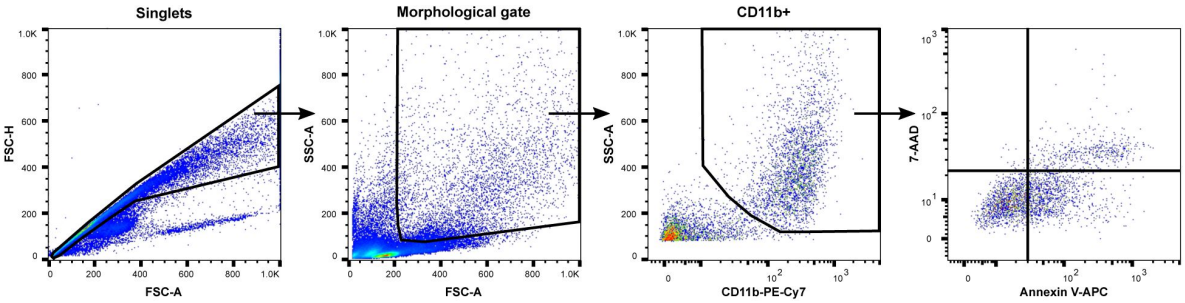

Figure 4—figure supplement 2.

MTBC strains did not induce significantly different percentages of necrotic macrophages.

Percentage of necrotic macrophages (CD11b$^+$ Annexin V$^+$ 7-AAD$^+$) on day 6 post-infection quantified by flow cytometry. Colors indicate lineage, bars represent medians, and shapes stand for independent donors (n = 4). Statistical analysis by Friedman test.

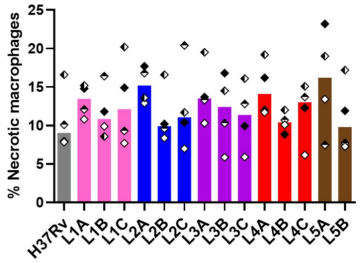

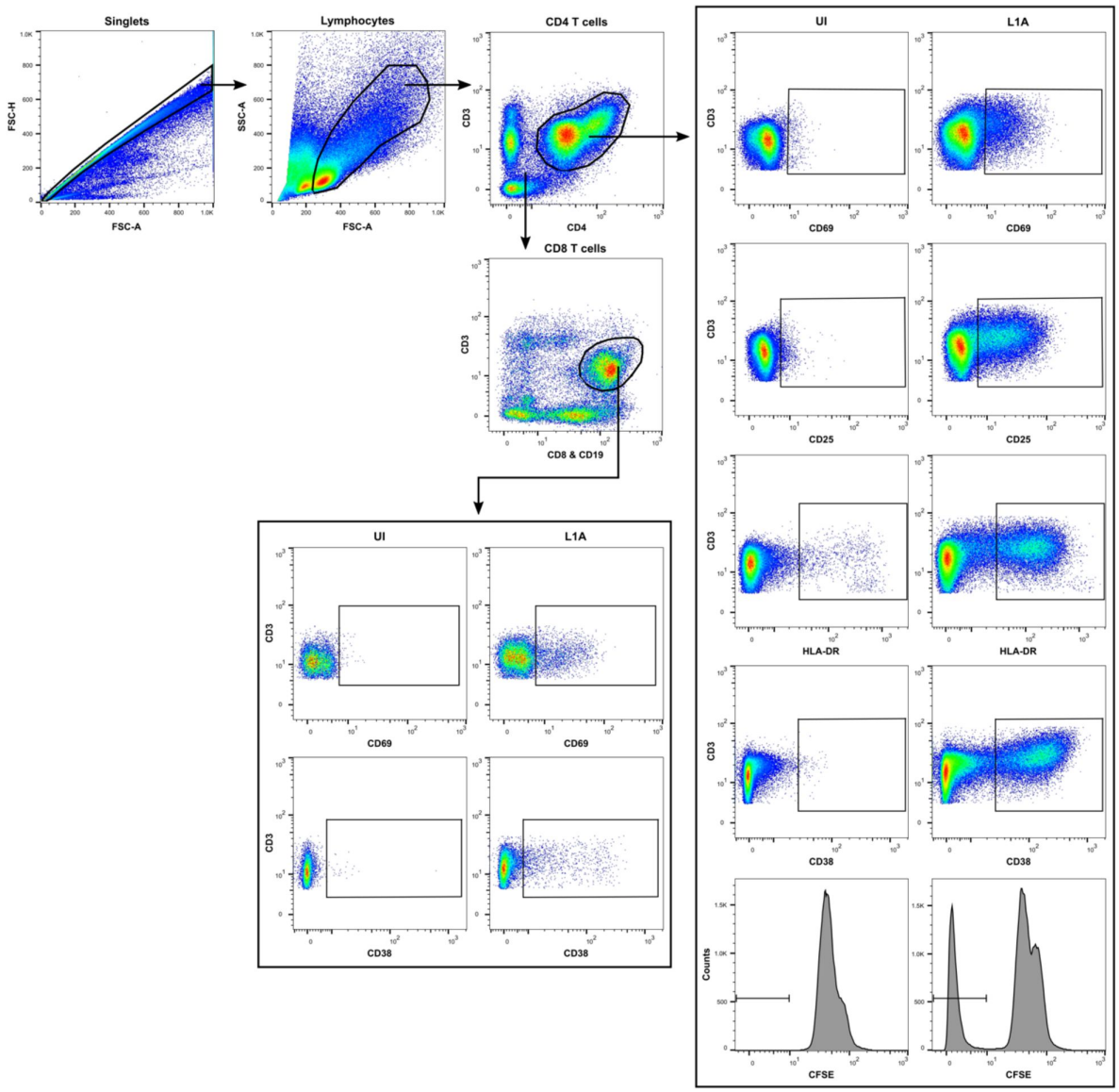

Figure 5—figure supplement 1.

Flow cytometry gating strategy for the analysis of T cell proliferation and activation.

UI, uninfected.

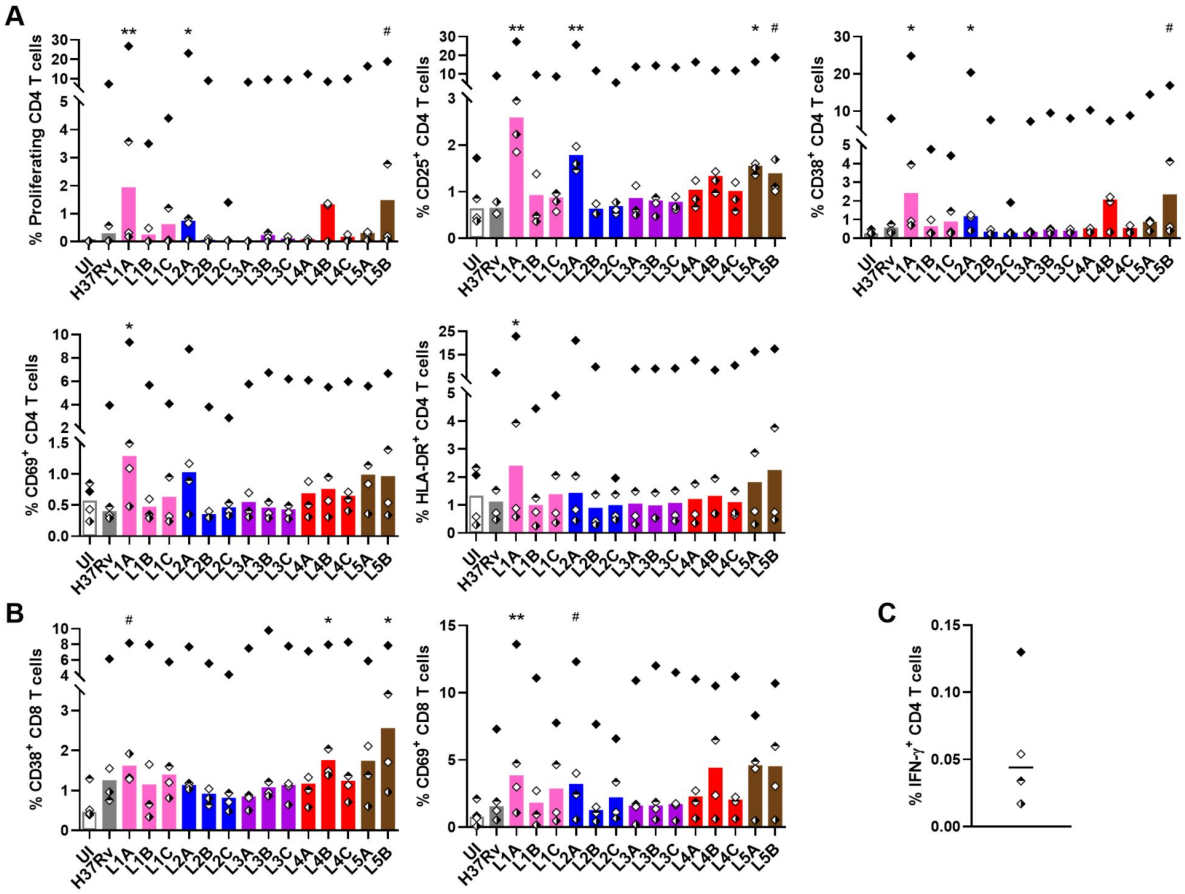

Figure 5—figure supplement 2.

MTBC strain diversity results in induction of quantitatively distinct T cell responses.

Frequencies of **(A)** proliferating and/or activated CD4 and **(B)** CD8 T cells quantified by flow cytometry on day 6 post-infection. UI, uninfected. Colors indicate lineage, shapes correspond to individual donors (n = 4) and bars represent medians. Statistical analysis by Friedman test with *post hoc* Dunn's correction (comparisons against UI). #, $p < 0.1$; *, $p < 0.05$; **, $p < 0.01$. **(C)** Frequency of IFN-ψ^+ CD4 T cells quantified by flow cytometry upon overnight PPD stimulation. Shapes same as in (**A-B**) and horizontal line represents the median.

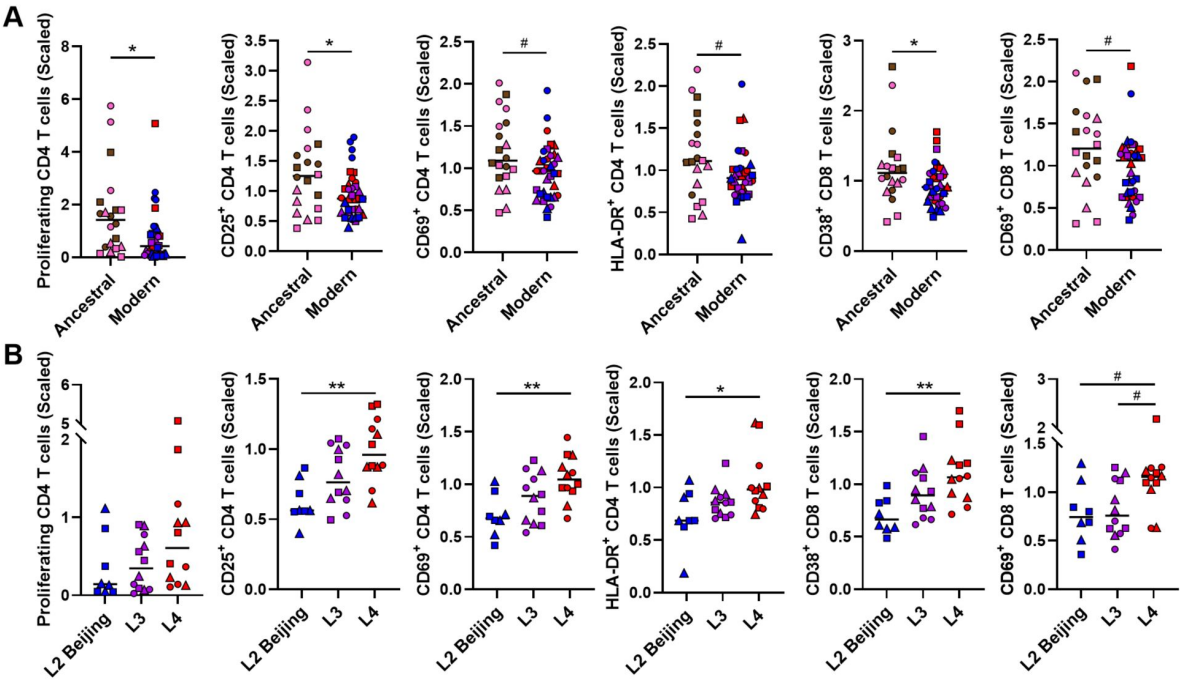

Figure 5—figure supplement 3.

Induction of T cell activation and proliferation exhibits both lineage- and mycobacterial growth-associated trends.

Frequency of each population stratified by **(A)** ancestral or modern lineage, or **(B)** specific modern lineages. Statistical analyses by (**A**) two-tailed Mann-Whitney or (**B**) Kruskal-Wallis test with *post hoc* Dunn's correction. * $p < 0.05$; **, $p < 0.01$. Colors indicate lineage, shapes stand for individual strains within the same lineage (LXA in circles, LXB in squares and LXC in triangles) and horizontal lines represent medians.

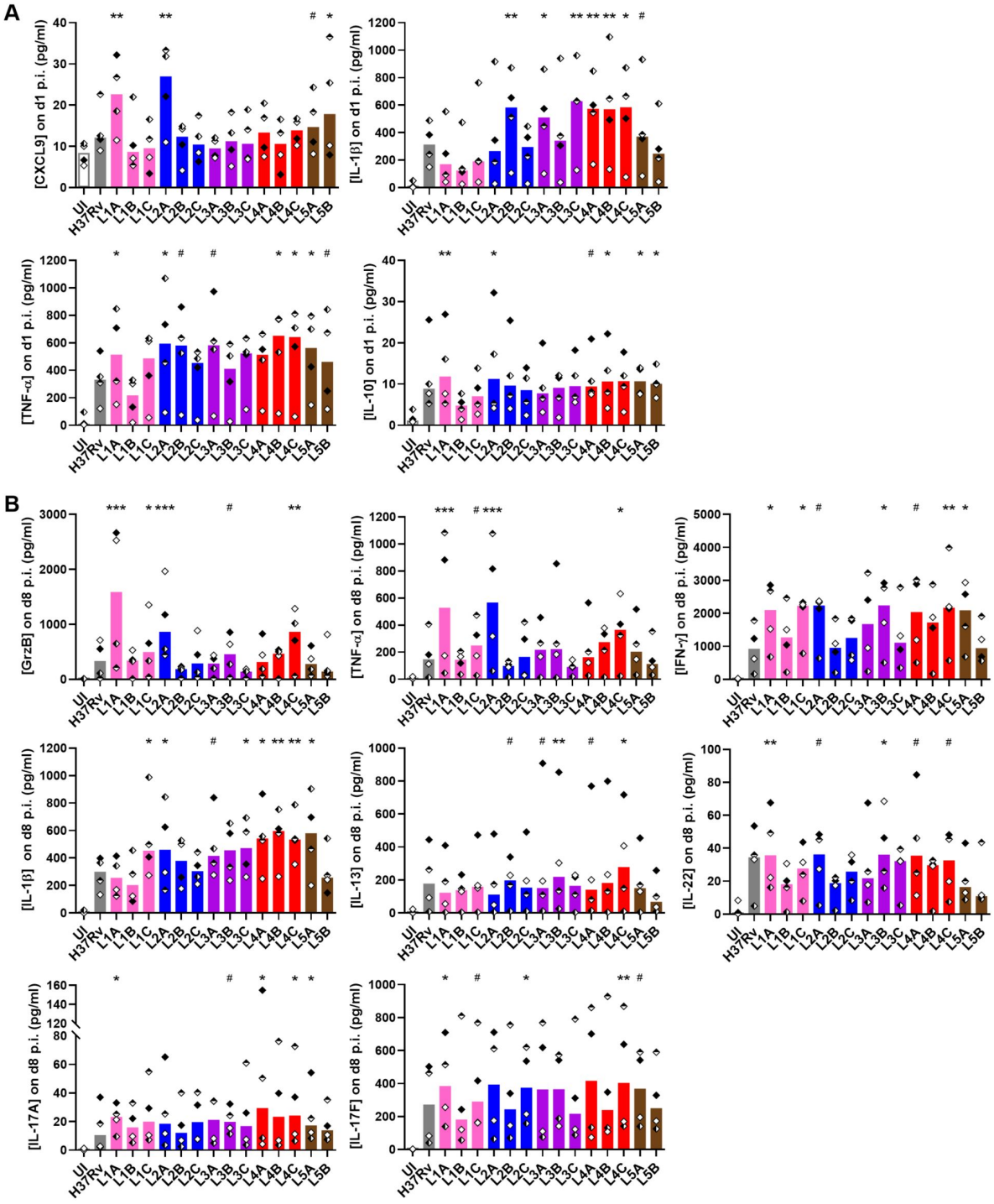

Figure 6—figure supplement 1.

MTBC diversity results in variable soluble factor immune responses.

Concentrations of soluble factors induced by MTBC infection on **(A)** day 1 or **(B)** day 8 post-infection (p.i). UI, uninfected. Colors indicate lineage, shapes stand for independent donors (n = 4), and bars represent medians. Statistical analysis by Friedman test with *post hoc* Dunn's correction (comparisons against UI). #, $p < 0.1$; *, $p < 0.05$; **, $p < 0.01$; $p < 0.001$.

References

1. Aguilo J.I., Alonso H., Uranga S., Marinova D., Arbues A., de Martino A., Anel A., Monzon M., Badiola J., Pardo J., et al. 2013) **ESX-1-induced apoptosis is involved in cell-to-cell spread of Mycobacterium tuberculosis** *Cell Microbiol* **15**:1994–2005

2. Ambreen A., Khaliq A., Naqvi S.Z.H., Tahir A., Mustafa M., Chaudhary S.U., Mirza S., Mustafa T. 2021) **Host biomarkers for monitoring therapeutic response in extrapulmonary tuberculosis** *Cytokine* **142**

3. Andrews J.T., Zhang Z., Prasad G., Huey F., Nazarova E.V., Wang J., Ranaraja A., Weinkopff T., Li L.X., Mu S., et al. 2024) **Metabolically active neutrophils represent a permissive niche for Mycobacterium tuberculosis** *Mucosal Immunol*

4. Arbues A., Brees D., Chibout S.D., Fox T., Kammuller M., Portevin D. 2020a) **TNF-alpha antagonists differentially induce TGF-beta1-dependent resuscitation of dormant-like Mycobacterium tuberculosis** *PLoS Pathog* **16**

5. Arbues A., Kammuller M., Portevin D. 2020b) **Generating Three-dimensional Human Granulomas in vitro to Study Mycobacterium tuberculosis-Host Interaction** *Bio Protoc* **10**

6. Arbues A., Schmidiger S., Kammuller M., Portevin D. 2021) **Extracellular Matrix-Induced GM-CSF and Hypoxia Promote Immune Control of Mycobacterium tuberculosis in Human In Vitro Granulomas** *Front Immunol* **12**

7. Asante-Poku A., Yeboah-Manu D., Otchere I.D., Aboagye S.Y., Stucki D., Hattendorf J., Borrell S., Feldmann J., Danso E., Gagneux S. 2015) **Mycobacterium africanum is associated with patient ethnicity in Ghana** *PLoS Negl Trop Dis* **9**

8. Ates L.S., Dippenaar A., Sayes F., Pawlik A., Bouchier C., Ma L., Warren R.M., Sougakoff W., Majlessi L., van Heijst J.W.J., et al. 2018) **Unexpected Genomic and Phenotypic Diversity of Mycobacterium africanum Lineage 5 Affects Drug Resistance, Protein Secretion, and Immunogenicity** *Genome Biol Evol* **10**:1858–1874

9. Borrell S., Trauner A., Brites D., Rigouts L., Loiseau C., Coscolla M., Niemann S., De Jong B., Yeboah-Manu D., Kato-Maeda M., et al. 2019) **Reference set of Mycobacterium tuberculosis clinical strains: A tool for research and product development** *PLoS One* **14**

10. Bottai D., Frigui W., Sayes F., Di Luca M., Spadoni D., Pawlik A., Zoppo M., Orgeur M., Khanna V., Hardy D., et al. 2020) **TbD1 deletion as a driver of the evolutionary success of modern epidemic Mycobacterium tuberculosis lineages** *Nat Commun* **11**

11. Brosch R., Gordon S.V., Marmiesse M., Brodin P., Buchrieser C., Eiglmeier K., Garnier T., Gutierrez C., Hewinson G., Kremer K., et al. 2002) **A new evolutionary scenario for the Mycobacterium tuberculosis complex** *Proc Natl Acad Sci U S A* **99**:3684–3689

12. Caws M., Thwaites G., Dunstan S., Hawn T.R., Lan N.T., Thuong N.T., Stepniewska K., Huyen M.N., Bang N.D., Loc T.H., et al. 2008) **The influence of host and bacterial genotype on the development of disseminated disease with Mycobacterium tuberculosis** *PLoS Pathog* **4**

13. Click E.S., Moonan P.K., Winston C.A., Cowan L.S., Oeltmann J.E. 2012) **Relationship between Mycobacterium tuberculosis phylogenetic lineage and clinical site of tuberculosis** *Clin Infect Dis* **54**:211–219

14. Coll F., McNerney R., Guerra-Assuncao J.A., Glynn J.R., Perdigao J., Viveiros M., Portugal I., Pain A., Martin N., Clark T.G. 2014) **A robust SNP barcode for typing Mycobacterium tuberculosis complex strains** *Nat Commun* **5**

15. Comas I., Coscolla M., Luo T., Borrell S., Holt K.E., Kato-Maeda M., Parkhill J., Malla B., Berg S., Thwaites G., et al. 2013) **Out-of-Africa migration and Neolithic coexpansion of Mycobacterium tuberculosis with modern humans** *Nat Genet* **45**:1176–1182

16. Coscolla M., Gagneux S., Menardo F., Loiseau C., Ruiz-Rodriguez P., Borrell S., Otchere I.D., Asante-Poku A., Asare P., Sanchez-Buso L., et al. 2021) **Phylogenomics of Mycobacterium africanum reveals a new lineage and a complex evolutionary history** *Microb Genom* **7**

17. Davis J.M., Ramakrishnan L. 2009) **The role of the granuloma in expansion and dissemination of early tuberculous infection** *Cell* **136**:37–49

18. Domenech P., Kolly G.S., Leon-Solis L., Fallow A., Reed M.B. 2010) **Massive gene duplication event among clinical isolates of the Mycobacterium tuberculosis W/Beijing family** *J Bacteriol* **192**:4562–4570

19. Domenech P., Zou J., Averback A., Syed N., Curtis D., Donato S., Reed M.B. 2017) **Unique Regulation of the DosR Regulon in the Beijing Lineage of Mycobacterium tuberculosis** *J Bacteriol* **199**

20. Esaulova E., Das S., Singh D.K., Choreno-Parra J.A., Swain A., Arthur L., Rangel-Moreno J., Ahmed M., Singh B., Gupta A., et al. 2021) **The immune landscape in tuberculosis reveals populations linked to disease and latency** *Cell Host Microbe* **29**:165–178

21. Flynn J.L., Goldstein M.M., Chan J., Triebold K.J., Pfeffer K., Lowenstein C.J., Schreiber R., Mak T.W., Bloom B.R. 1995) **Tumor necrosis factor-alpha is required in the protective immune response against Mycobacterium tuberculosis in mice** *Immunity* **2**:561–572

22. Fong Y., Sebestyen K., Yu X., Gilbert P., Self S. 2013) **nCal: an R package for non-linear calibration** *Bioinformatics* **29**:2653–2654

23. Gagneux S., DeRiemer K., Van T., Kato-Maeda M., de Jong B.C., Narayanan S., Nicol M., Niemann S., Kremer K., Gutierrez M.C., et al. 2006) **Variable host-pathogen compatibility in Mycobacterium tuberculosis** *Proc Natl Acad Sci U S A* **103**:2869–2873

24. Garton N.J., Waddell S.J., Sherratt A.L., Lee S.M., Smith R.J., Senner C., Hinds J., Rajakumar K., Adegbola R.A., Besra G.S., et al. 2008) **Cytological and transcript analyses reveal fat and lazy persister-like bacilli in tuberculous sputum** *PLoS Med* **5**

25. Gehre F., Otu J., DeRiemer K., de Sessions P.F., Hibberd M.L., Mulders W., Corrah T., de Jong B.C., Antonio M. 2013) **Deciphering the growth behaviour of Mycobacterium africanum** *PLoS Negl Trop Dis* **7**

26. Gengenbacher M., Kaufmann S.H. 2012) **Mycobacterium tuberculosis: success through dormancy** *FEMS Microbiol Rev* **36**:514–532

27. Gideon H.P., Hughes T.K., Tzouanas C.N., Wadsworth M.H., Tu A.A., Gierahn T.M., Peters J.M., Hopkins F.F., Wei J.R., Kummerlowe C., et al. 2022) **Multimodal profiling of lung granulomas in macaques reveals cellular correlates of tuberculosis control** *Immunity* **55**:827–846

28. Gideon H.P., Phuah J., Junecko B.A., Mattila J.T. 2019) **Neutrophils express pro- and anti-inflammatory cytokines in granulomas from Mycobacterium tuberculosis-infected cynomolgus macaques** *Mucosal Immunol* **12**:1370–1381

29. Groom J.R., Luster A.D. 2011) **CXCR3 ligands: redundant, collaborative and antagonistic functions** *Immunol Cell Biol* **89**:207–215

30. Guerra-Assuncao J.A., Crampin A.C., Houben R.M., Mzembe T., Mallard K., Coll F., Khan P., Banda L., Chiwaya A., Pereira R.P., et al. 2015) **Large-scale whole genome sequencing of M. tuberculosis provides insights into transmission in a high prevalence area** *Elife* **4**

31. Guyeux C., Senelle G., Le Meur A., Supply P., Gaudin C., Phelan J.E., Clark T.G., Rigouts L., de Jong B., Sola C., et al. 2024) **Newly Identified Mycobacterium africanum Lineage 10, Central Africa** *Emerg Infect Dis* **30**:560–563

32. Hiza H., Zwyer M., Hella J., Arbués A., Sasamalo M., Borrell S., Xu Z.M., Ross A., Brites D., Fellay J., et al. 2023) **Bacterial diversity dominates variable macrophage responses of tuberculosis patients in Tanzania** *bioRxiv*

33. Issafras H., Corbin J.A., Goldfine I.D., Roell M.K. 2014) **Detailed mechanistic analysis of gevokizumab, an allosteric anti-IL-1beta antibody with differential receptor-modulating properties** *J Pharmacol Exp Ther* **348**:202–215

34. Joosten S.A., van Meijgaarden K.E., Arend S.M., Prins C., Oftung F., Korsvold G.E., Kik S.V., Arts R.J., van Crevel R., Netea M.G., et al. 2018) **Mycobacterial growth inhibition is associated with trained innate immunity** *J Clin Invest* **128**:1837–1851

35. Kaufmann S.H. 2002) **Protection against tuberculosis: cytokines, T cells, and macrophages** *Ann Rheum Dis* **61**:ii54–58

36. Khader S.A., Bell G.K., Pearl J.E., Fountain J.J., Rangel-Moreno J., Cilley G.E., Shen F., Eaton S.M., Gaffen S.L., Swain S.L., et al. 2007) **IL-23 and IL-17 in the establishment of protective pulmonary CD4+ T cell responses after vaccination and during Mycobacterium tuberculosis challenge** *Nat Immunol* **8**:369–377

37. Lovey A., Verma S., Kaipilyawar V., Ribeiro-Rodrigues R., Husain S., Palaci M., Dietze R., Ma S., Morrison R.D., Sherman D.R., et al. 2022) **Early alveolar macrophage response and IL-1R-dependent T cell priming determine transmissibility of Mycobacterium tuberculosis strains** *Nat Commun* **13**

38. Lowe D.M., Bandara A.K., Packe G.E., Barker R.D., Wilkinson R.J., Griffiths C.J., Martineau A.R. 2013) **Neutrophilia independently predicts death in tuberculosis** *Eur Respir J* **42**:1752–1757

39. Manca C., Tsenova L., Barry C.E., Bergtold A., Freeman S., Haslett P.A., Musser J.M., Freedman V.H., Kaplan G. 1999) **Mycobacterium tuberculosis CDC1551 induces a more vigorous host response in vivo and in vitro, but is not more virulent than other clinical isolates** *J Immunol* **162**:6740–6746

40. Manca C., Tsenova L., Bergtold A., Freeman S., Tovey M., Musser J.M., Barry C.E., Freedman V.H., Kaplan G. 2001) **Virulence of a Mycobacterium tuberculosis clinical isolate in mice is**

determined by failure to induce Th1 type immunity and is associated with induction of IFN-alpha/beta *Proc Natl Acad Sci U S A* **98**:5752–5757

41. Mayer-Barber K.D., Barber D.L., Shenderov K., White S.D., Wilson M.S., Cheever A., Kugler D., Hieny S., Caspar P., Nunez G., et al. 2010) **Caspase-1 independent IL-1beta production is critical for host resistance to mycobacterium tuberculosis and does not require TLR signaling in vivo** *J Immunol* **184**:3326–3330

42. Mitchison D.A., Wallace J.G., Bhatia A.L., Selkon J.B., Subbaiah T.V., Lancaster M.C. 1960) **A comparison of the virulence in guinea-pigs of South Indian and British tubercle bacilli** *Tubercle* **41**:1–22

43. Moreira-Teixeira L., Tabone O., Graham C.M., Singhania A., Stavropoulos E., Redford P.S., Chakravarty P., Priestnall S.L., Suarez-Bonnet A., Herbert E., et al. 2020) **Mouse transcriptome reveals potential signatures of protection and pathogenesis in human tuberculosis** *Nat Immunol* **21**:464–476

44. Napier G., Campino S., Merid Y., Abebe M., Woldeamanuel Y., Aseffa A., Hibberd M.L., Phelan J., Clark T.G. 2020) **Robust barcoding and identification of Mycobacterium tuberculosis lineages for epidemiological and clinical studies** *Genome Med* **12**

45. Nebenzahl-Guimaraes H., Verhagen L.M., Borgdorff M.W., van Soolingen D. 2015) **Transmission and Progression to Disease of Mycobacterium tuberculosis Phylogenetic Lineages in The Netherlands** *J Clin Microbiol* **53**:3264–3271

46. Netikul T., Palittapongarnpim P., Thawornwattana Y., Plitphonganphim S. 2021) **Estimation of the global burden of Mycobacterium tuberculosis lineage 1** *Infect Genet Evol* **91**

47. Newton S.M., Smith R.J., Wilkinson K.A., Nicol M.P., Garton N.J., Staples K.J., Stewart G.R., Wain J.R., Martineau A.R., Fandrich S., et al. 2006) **A deletion defining a common Asian lineage of Mycobacterium tuberculosis associates with immune subversion** *Proc Natl Acad Sci U S A* **103**:15594–15598

48. Ofori-Anyinam B., Dolganov G., Van T., Davis J.L., Walter N.D., Garcia B.J., Voskuil M., Fissette K., Diels M., Driesen M., et al. 2017) **Significant under expression of the DosR regulon in M. tuberculosis complex lineage 6 in sputum** *Tuberculosis (Edinb* **104**:58–64

49. Osei-Wusu S., Tetteh J.K.A., Musah A.B., Ntiamoah D.O., Arthur N., Adjei A., Arbues A., Ofori E.A., Mensah K.A., Galevo S.E.A., et al. 2023) **Macrophage susceptibility to infection by Ghanaian Mycobacterium tuberculosis complex lineages 4 and 5 varies with self-reported ethnicity** *Front Cell Infect Microbiol* **13**

50. Pagan A.J., Ramakrishnan L. 2014) **Immunity and Immunopathology in the Tuberculous Granuloma** *Cold Spring Harb Perspect Med* **5**

51. Perez I., Uranga S., Sayes F., Frigui W., Samper S., Arbues A., Aguilo N., Brosch R., Martin C., Gonzalo-Asensio J. 2020) **Live attenuated TB vaccines representing the three modern Mycobacterium tuberculosis lineages reveal that the Euro-American genetic background confers optimal vaccine potential** *EBioMedicine* **55**

52. Plumlee C.R., Duffy F.J., Gern B.H., Delahaye J.L., Cohen S.B., Stoltzfus C.R., Rustad T.R., Hansen S.G., Axthelm M.K., Picker L.J., et al. 2021) **Ultra-low Dose Aerosol Infection of Mice with Mycobacterium tuberculosis More Closely Models Human Tuberculosis** *Cell Host Microbe* **29**:68–82

53. Poonawala H., Kumar N., Peacock S.J. 2020) **A review of published spoligotype data indicates the diversity of Mycobacterium tuberculosis from India is under-represented in global databases** *Infect Genet Evol* **78**

54. Portevin D., Gagneux S., Comas I., Young D. 2011) **Human macrophage responses to clinical isolates from the Mycobacterium tuberculosis complex discriminate between ancient and modern lineages** *PLoS Pathog* **7**

55. Reed M.B., Domenech P., Manca C., Su H., Barczak A.K., Kreiswirth B.N., Kaplan G., Barry C.E. 2004) **A glycolipid of hypervirulent tuberculosis strains that inhibits the innate immune response** *Nature* **431**:84–87

56. Reed M.B., Gagneux S., Deriemer K., Small P.M., Barry C.E. 2007) **The W-Beijing lineage of Mycobacterium tuberculosis overproduces triglycerides and has the DosR dormancy regulon constitutively upregulated** *J Bacteriol* **189**:2583–2589

57. Reiling N., Homolka S., Walter K., Brandenburg J., Niwinski L., Ernst M., Herzmann C., Lange C., Diel R., Ehlers S., et al. 2013) **Clade-specific virulence patterns of Mycobacterium tuberculosis complex strains in human primary macrophages and aerogenically infected mice** *mBio* **4**

58. Ribeiro S.C., Gomes L.L., Amaral E.P., Andrade M.R., Almeida F.M., Rezende A.L., Lanes V.R., Carvalho E.C., Suffys P.N., Mokrousov I., et al. 2014) **Mycobacterium tuberculosis strains of the modern sublineage of the Beijing family are more likely to display increased virulence than strains of the ancient sublineage** *J Clin Microbiol* **52**:2615–2624

59. Romagnoli A., Petruccioli E., Palucci I., Camassa S., Carata E., Petrone L., Mariano S., Sali M., Dini L., Girardi E., et al. 2018) **Clinical isolates of the modern Mycobacterium tuberculosis lineage 4 evade host defense in human macrophages through eluding IL-1beta-induced autophagy** *Cell Death Dis* **9**

60. Saelens J.W., Sweeney M.I., Viswanathan G., Xet-Mull A.M., Jurcic Smith K.L., Sisk D.M., Hu D.D., Cronin R.M., Hughes E.J., Brewer W.J., et al. 2022) **An ancestral mycobacterial effector promotes dissemination of infection** *Cell* **185**:4507–4525

61. Seraphin M.N., Doggett R., Johnston L., Zabala J., Gerace A.M., Lauzardo M. 2017) **Association between Mycobacterium tuberculosis lineage and site of disease in Florida, 2009-2015** *Infect Genet Evol* **55**:366–371

62. Shanmugasundaram U., Bucsan A.N., Ganatra S.R., Ibegbu C., Quezada M., Blair R.V., Alvarez X., Velu V., Kaushal D., Rengarajan J. 2020) **Pulmonary Mycobacterium tuberculosis control associates with CXCR3- and CCR6-expressing antigen-specific Th1 and Th17 cell recruitment** *JCI Insight* **5**

63. Sigal G.B., Segal M.R., Mathew A., Jarlsberg L., Wang M., Barbero S., Small N., Haynesworth K., Davis J.L., Weiner M., et al. 2017) **Biomarkers of Tuberculosis Severity and Treatment Effect: A Directed Screen of 70 Host Markers in a Randomized Clinical Trial** *EBioMedicine* **25**:112–121

64. Silva M.L., Ca B., Osorio N.S., Rodrigues P.N.S., Maceiras A.R., Saraiva M. 2022) **Tuberculosis caused by Mycobacterium africanum: Knowns and unknowns** *PLoS Pathog* **18**

65. Tameris M., McShane H., McClain J.B., Landry B., Lockhart S., Luabeya A.K., Geldenhuys H., Shea J., Hussey G., van der Merwe L., et al. 2013) **Lessons learnt from the first efficacy trial of a**

new infant tuberculosis vaccine since BCG *Tuberculosis (Edinb* **93**:143–149

66. Tezera L.B., Bielecka M.K., Ogongo P., Walker N.F., Ellis M., Garay-Baquero D.J., Thomas K., Reichmann M.T., Johnston D.A., Wilkinson K.A., et al. 2020) **Anti-PD-1 immunotherapy leads to tuberculosis reactivation via dysregulation of TNF-alpha** *Elife* **9**

67. Thacker V.V., Dhar N., Sharma K., Barrile R., Karalis K., McKinney J.D. 2020) **A lung-on-chip model of early Mycobacterium tuberculosis infection reveals an essential role for alveolar epithelial cells in controlling bacterial growth** *Elife* **9**

68. Tram T.T.B., Nhung H.N., Vijay S., Hai H.T., Thu D.D.A., Ha V.T.N., Dinh T.D., Ashton P.M., Hanh N.T., Phu N.H., et al. 2018) **Virulence of Mycobacterium tuberculosis Clinical Isolates Is Associated With Sputum Pre-treatment Bacterial Load, Lineage, Survival in Macrophages, and Cytokine Response** *Front Cell Infect Microbiol* **8**

69. Tsao T.C., Hong J., Li L.F., Hsieh M.J., Liao S.K., Chang K.S. 2000) **Imbalances between tumor necrosis factor-alpha and its soluble receptor forms, and interleukin-1beta and interleukin-1 receptor antagonist in BAL fluid of cavitary pulmonary tuberculosis** *Chest* **117**:103–109

70. Tsenova L., Ellison E., Harbacheuski R., Moreira A.L., Kurepina N., Reed M.B., Mathema B., Barry C.E., Kaplan G. 2005) **Virulence of selected Mycobacterium tuberculosis clinical isolates in the rabbit model of meningitis is dependent on phenolic glycolipid produced by the bacilli** *J Infect Dis* **192**:98–106

71. Uzorka J.W., Bakker J.A., van Meijgaarden K.E., Leyten E.M.S., Delfos N.M., Hetem D.J., Kerremans J., Zwarts M., Cozijn S., Ottenhoff T.H.M., et al. 2022) **Biomarkers to identify Mycobacterium tuberculosis infection among borderline QuantiFERON results** *Eur Respir J* **60**

72. Wang C., Peyron P., Mestre O., Kaplan G., van Soolingen D., Gao Q., Gicquel B., Neyrolles O. 2010) **Innate immune response to Mycobacterium tuberculosis Beijing and other genotypes** *PLoS One* **5**

73. Wang J., Fan X.Y., Hu Z. 2024) **Immune correlates of protection as a game changer in tuberculosis vaccine development** *NPJ Vaccines* **9**

74. WHO 2023) **Global Tuberculosis Report 2023** WHO

Author information

Ainhoa Arbués[#]
Swiss Tropical and Public Health Institute, Allschwil, Switzerland, University of Basel, Basel, Switzerland

[#]Current address: Departamento de Microbiología, Pediatría, Radiología y Salud Pública, Facultad de Medicina, Universidad de Zaragoza, Zaragoza, Spain.

Sarah Schmidiger
Swiss Tropical and Public Health Institute, Allschwil, Switzerland, University of Basel, Basel, Switzerland

Miriam Reinhard
Swiss Tropical and Public Health Institute, Allschwil, Switzerland, University of Basel, Basel, Switzerland

Sònia Borrell
Swiss Tropical and Public Health Institute, Allschwil, Switzerland, University of Basel, Basel, Switzerland

Sébastien Gagneux
Swiss Tropical and Public Health Institute, Allschwil, Switzerland, University of Basel, Basel, Switzerland

Damien Portevin
Swiss Tropical and Public Health Institute, Allschwil, Switzerland, University of Basel, Basel, Switzerland
ORCID iD: 0000-0003-2949-9557

For correspondence: damien.portevin@swisstph.ch

Editors

Reviewer #2 (Public review):

Summary:

This manuscript reports a comparison of microbial traits and host response traits in a laboratory model of infected granuloma using Mtb strains from different lineages. The authors report increased bacillary growth and granuloma formation, inversely associated with T cell activation that is characterized by CXCL9, granzyme B and TNF expression. They therefore infer that these T cell responses are likely to be host-protective and that the greater virulence of modern Mtb lineages may be driven by their ability to avoid triggering these responses.

Strengths:

The comparison of multiple Mtb lineages in a granuloma model that enables evaluation of the potential role of multiple host cells in Mtb control, offers a valuable experimental approach to study the biological mechanisms that underpin differential virulence of Mtb lineages that has been previously reported in clinical and epidemiological studies.

Weaknesses:

The study is rather limited to descriptive observations, and lacks experiments to test causal relationships between host and pathogen traits. Some of the presentation of the data are difficult to interpret, and some conclusions are not adequately supported by the data.

Comments on revisions:

The authors have addressed my previous comments with appropriate revisions and explanations.

https://doi.org/10.7554/eLife.99062.2.sa2

Reviewer #3 (Public review):

Arbués and colleagues describe the impact of mycobacterial genetic diversity on host-infection phenotypes. The authors evaluate Mtb infection and contextualize host-responses, bacterial growth and metabolic transitioning in vitro using their previously established model of blood-derived, primary-human-cells cultured within a collagen/fibronectin matrix. They seek to demonstrate the effectiveness of the model in determining mycobacterial strain specific granuloma-dependent host-pathogen interactions.

Understanding the way mycobacterial genetic diversity impacts granuloma biology in tuberculosis is an important goal. One of this works strengths is the use of primary human cells and two constituents of pulmonary extracellular matrix to model Mtb infection. The authors and others have previously shown that Mtb infected PBMC aggregates share important characteristics with early pulmonary TB granulomas. Use of multiple genetically distinct strains of Mtb defines this work and further bolsters it potential impact. However, the study is not comprehensive as lineages 6 and 7 are not tested. Experiments are primarily descriptive, and the methodologies are conventional. Correlative relationships are the manuscripts focus and effect sizes are generally small.

The main aim of this work is to extend an in vitro granuloma model to the study of a large collection of well characterized, genetically diverse representatives of the mycobacterium tuberculosis complex (MTBC). I believe that they accomplish that aim. The work does investigate MTBC infection of aggregated PBMCs using three strains each of Mtb lineages 1-5 and H37Rv, which is not a trivial undertaking. The experimental aims are to show that MTBC genetic diversity impacts growth and dormancy of granuloma bound bacteria and, the host responses of granulomatous aggregation as well as macrophage apoptosis, lymphocyte activation and soluble mediator release within granulomas. The methodologies employed are sufficient to test most of these aims. The authors conclusions regarding their results are mostly supported by the data. The conclusion that lineage impacts growth within granulomas is likely true and the data as presented reflect such a relationship. Their conclusions regarding lineage's impact on dormancy are partially supported, as their findings demonstrate that assays for dormancy identify strain-specific metabolic changes in the bacteria consistent with a dormancy-like state but also identify replicating bacteria as being dormant. The data strongly supports the impact of mycobacterial genetic diversity on a spectrum of granulomatous responses in their model system. Those findings are a highlight of the publication. The data further supports the idea that strain diversity impacts macrophage apoptosis but a relationship of apoptosis to the granulomatous response is not effectively evaluated. The association of lymphocyte activation with reduced mycobacterial growth as an aspect of granulomas is well documented in the literature and a negative correlation between T cell activation and growth is supported by the authors results. Their data also support the conclusion that soluble mediator production by PBMCs is different based on the infecting strain of mycobacteria and that IL1b modulates aggregate phenotypes in their model.

The authors contribute some valuable insights, particularly in figure 3. Their model is higher echelon relative to others in the field, but I don't believe that it possesses all the components necessary to replicate formation of mycobacterial granulomas in vivo. That being said, their identification of donor-dependent aggregation phenotypes by mycobacterial strain has the potential to enable future investigations of human and mycobacterial genetic components that are involved in the formation of TB granulomas.

https://doi.org/10.7554/eLife.99062.2.sa1

Author response:

The following is the authors' response to the original reviews.

> ***Reviewer #1:***
>
> *The analysis of the dormancy rates is interesting and offers some intriguing questions related to the higher dormancy rate found for the L2 isolates and lower for the L3 ones. It will be interesting in the future to expand the data generated in this advanced in vitro plaAorm to in vivo studies.*

Indeed, an increased dormancy propensity of L2 isolates was previously reported in broth culture and associated to specific genetic polymorphisms. The opposite phenotype observed in the L3 isolates is indeed particularly intriguing and was not described to date. Hence, we fully agree that it would be very interesting to find out whether these phenotypes are also observed in vivo.

> *The authors propose that 'strains exhibiting greater proliferative capacity are more prone to induce macrophage apoptosis, thereby contributing to the extent of the granulomatous response.' It would be interesting to know what happens if the macrophage apoptotic response is blocked.*

This is an interesting suggestion that would deserve a dedicated comprehensive investigation covering other cell death pathways. Even though the trend is significant, the correlation coefficient is rather low in this interaction, which looks *a fortiori* due to substantial inter-host variability in the apoptotic propensity of macrophages from individual donors to a given strain. In addition, such blocking experiments may require performing isolated macrophage infections that would fall outside of the scope of this study, or considering the extent and the contribution of the apoptosis of other cell subsets.

> *In contrast to macrophage apoptosis, T cell activation correlated with less replicative bacteria. Are these two findings related, ie, are the granulomas showing more (apoptotic) macrophages the ones with a lower percentage of activated T cells? This would shed light on what distinguishes granulomas that are protective from those that support bacterial growth.*

Indeed, a significant negative correlation between macrophage apoptosis induction and T cell activation can be observed, specifically with activated CD4 T cells expressing CD38 ($rS = -0.36$, $p < 0.05$) or CD69 ($rS = -0.40$, $p < 0.01$). We have added this additional result in the manuscript text (line 217).

> *It would also be interesting to know the functional impact of blocking early CXCL9 or IL1b on the outcome of granulomatous response/bacteria growth.*

We have performed the suggested early blocking experiments and added the expected negative effect on granuloma formation upon neutralization of IL-1b (current Fig. 6E) in the revised version of the manuscript, and furthermore discussed the null effect on bacterial growth of the treatment with an anti-CXCL-9 specific antibody (current Fig. 6H).

> *The authors acknowledge the absence of neutrophils in this model. However, this could be discussed in more detail, as neutrophils play an important part in TB pathogenesis as shown in different models of infection and human TB.*

We concur and have expanded the importance of neutrophils in TB pathogenesis (including references) in the discussion section (line 260).

> *Related to neutrophils and TB pathogenesis, another important player is type I IFN. The multiplex assay used included IFN-alpha, was this molecule detected? If so, was there any difference in the levels of type I IFN detected among the different infections?*

We agree and that is why we had originally included IFN-α in our screen. However, this cytokine remained under the limit of quantification at both studied time points, preventing us to draw conclusions on the effect of *Mtb* strain diversity on the secretion of type I IFNs in *in vitro* granulomas.

> ***Reviewer #2:***
>
> *In Figure 1b/c, it is not clear what comparisons are being made to give the p-value annotations.*
>
> *In Figure 2a/b, it is not clear what comparisons are being made to give the p-value annotations.*
>
> *In Figure 3a, again it is not clear what comparisons are being made to give the p-value annotation.*

The *p*-values formerly present on the upper le] corner of the panels were resulting from either Friedman (Figures 1C, 2A and 3A) or Kruskal-Wallis (Figures 1B and 2B) tests and indicated whether there was a significant difference between the analyzed groups overall. To avoid confusion, those values have been removed to only leave the post-test comparison between specific groups.

> *In the results narrative related to Figure 1 (lines 93-103), the authors refer to lineage heterogeneity without providing any objective quantification of this - I suggest they do so, by providing variance or standard deviations.*

Thank you very much for this relevant suggestion, we have now included the coefficients of variation as a quantitative measure of the within-lineage heterogeneity in the manuscript (line 97).

> *I also suggest the authors explain what the data points actually represent in this figure - do I assume each data point = cfu from a well of 'granuloma'? Are they all from the same donor PBMC? What is the sample N for each lineage? If the data are not from the same donor PBMC, I think more informative to present the results of paired statistical analyses, stratified by donor cells. In addition, the authors should include a summary table of the demographic characteristics of the donors (at least sex, ethnicity, and age). If the data are derived from a single donor, I'd advocate providing data from at least one further donor.*

In the new supplementary figure requested by Reviewer 3 Figure 1—figure supplement 1 (actual CFU data on days 1 and 8 p.i. used to calculate the growth rate) it is now indicated that bacterial load was quantified as CFU per well.

Regarding the number of donors used, as stated in the Material and Methods section (current line 418) and depicted by the four different shapes used when data are grouped by individual infecting strain, all figures in our manuscript have been generated using PBMCs from 4 independent donors. For greater clarity, “n = 4” has now been included in the figure legends. Regarding the statistical analyses, paired statistical analyses stratified by donor were already performed in the original version of the manuscript whenever appropriate.

As stated in the methods section, the buffy coats used for PBMC isolation are anonymized so demographic data are unavailable.

> *The premise of the analysis in Figure tic and the results narrative ("This finding suggests that an increased ability to enter dormancy is not necessarily associated with a more pronounced growth phenotype", line 132) is not clear to me. Why would increased dormancy relate to increased growth in the same context? I suggest this analysis be removed.*

We apologize for the confusion in our original statement. We now rephrased it as “This finding suggests that an increased tendency to remain in a metabolically active state is not necessarily associated with a more pronounced growth phenotype”.

> *In Figure 3b, I think it may be more informative if the data points from the same donor were linked. Likewise in Figure 3c, I'd like to see a donor-paired statistical analysis.*

For all figures, the choice of using individual symbols to identify data points from the same donor but not connecting lines was made to provide a neater image. Nevertheless, we have now modified the figure linking the data points from the same donor. The statistical analysis performed is always donor-paired whenever appropriate.

> *The casual inference suggested in the results narrative between ‘macrophage apoptosis’ and granulomatous response line 173-175) is not tested directly by the experiment – I suggest the authors exclude this statement.*

Fair point, the statement has been removed.

> *To what extent have the authors considered whether variation in T cell responses between lineages may be confounded by variation in Mtb reactive T cell frequencies in donor PBMC. Can this be disentangled at all? This should be acknowledged as a potential limitation of the study.*

We did characterize the presence of mycobacterial antigen-specific reactive T cells in the PBMCs from the investigated donors. To do so, we performed *in vitro* stimulations with purified protein derivative (PPD) or an ESAT-6/CFP-10 peptide pool and quantified the frequency of IFN-γ-positive CD4 T cells by flow cytometry. The percentage of IFN-γg-positive CD4 T cells recalled by PPD stimulation ranged from 0.02% to 0.13%, while no ESAT6/CFP-10 reactive T cells were detected. As such, we can akest that the PBMC donors never encountered *Mtb* even though some levels of memory recalled by PPD may be due to cross-reactivity with BCG or pre-exposure to non-tuberculous mycobacteria. We have now added a panel in Figure 5—figure supplement 2 representing the frequency of mycobacteria-specific CD4 T cells and, as suggested, discussed the impact on the extent of the T cell responses observed in granulomas in the revised version of the manuscript. Nevertheless, the observed

MTBC strain-specific trends are consistent across the donors, as depicted in Figure 5B and Figure 5—figure supplement 2A-B.

> *Moreover, the experimental design does not really test cause and effect for the relationship between T cell proliferation/activation and bacterial growth. What is the impact of T-cell depletion from PBMC on bacterial growth?*

The increased TB susceptibility of HIV patients demonstrated that T cells play a critical part in the control of *Mtb* infection. We agree and did envisage such a depletion experiment. However, depleting T cells from PBMCs would imply removing up to 70% of the cells present in the specimen, which would lead to a situation from which results cannot be compared to the original sample and therefore would not be interpretable.

> ***Reviewer #3:***
>
> *Data presentation:*
>
> *- In Figure 1 (replication rate), actual cumulative CFU means from each strain for both days 1 and 8 with statistical analysis should be presented as panels in this figure.*

Agreed. We are providing the requested representation of the data and the corresponding paired statistical analysis as supplementary material Figure 1—figure supplement 1.

> *- In Figure 2 (dormancy), a panel comparing the mean number of bacteria that are single positive for either Auramine-O, Nile Red, or are double positive should be included for each strain, with statistical analysis. Representative photomicrographs of phenotypes from the staining should also be included. Electron microscopy could be conducted to compare the presence of intermediate lipid inclusions within organoidbound mycobacteria.*

As requested, percentages of single stained as well as double positive bacilli in each sample are now represented in Figure 2—figure supplement 1. In addition, we have now also followed the request and included a photomicrograph picturing representative *Mtb* staining phenotypes. Lastly, it would certainly be very elegant to visualize the presence of *Mtb* lipid inclusions within cellular aggregates by electron microscopy. However, we do not currently have the means for such investigations and the implementation of such a protocol under BSL3 conditions appears unrealistic in the context of this study.

> *- In Figure 3 (granulomatous response), the number, circularity, and size of immune aggregates are presented as "granuloma score" in which the mean ratio of size to circularity is divided by the number of inclusions. To their credit, in Supplementary Figure 2, the authors provide the data in a straighAorward manner. However, the granuloma score metric is reduced as the number of observed "granulomas" increases, which is counterintuitive. Additionally, circularity is not a definitive aspect of human granulomas (Wells et al., Am J Respir Crit Care Med, 2021, PMID: 34015247). I am skeptical that the "granuloma score" is an accurate predictor granulomatous inflammation. Is there precedent for this metric in the literature? If so, a reference should be provided. A high magnification inset of 1 representative granuloma from each strain should be included in Figure 3A.*

As requested, insets of a representative average granuloma for each strain have been included in Figure 3A. The formulation of the “granuloma score” has no precedent and cannot be referenced. By doing so, we meant to integrate within one single parameter the visual differences represented in the current Figure 3— figure supplement 2. We

intentionally sought to assign the highest score to the massive aggregation that some strains may promote unlike some that trigger several small, dispersed and diffused aggregates.

> *- In Figure 4 (macrophage apoptosis), a panel showing the percentage of dual Annexin V and 7-AAD positive cells should be included to provide the reader with the relative scope of ongoing apoptotic vs necrotic/secondary necrotic death in the model. If the data is readily available, including a control of uninfected PBMCs would also allow the reader to evaluate donor-dependent differences of in vitro cell death at baseline.*

No significant differences were observed in the percentage of dual Annexin V- and 7-AAD-positive macrophages (necrosis/secondary necrosis) between the MTBC strains at this time-point. Nevertheless, we have disclosed this result in the revised manuscript as Figure 4—figure supplement 2.

> *- In Figures 5 and 6 (lymphocyte activation and soluble mediator secretion), panels showing unscaled data should be included. Panels depicting the unscaled immunoassay protein readings (pg/mL) by strain for CXCL9, granzyme B, and TNF with statistical analysis should be included in Figure 6.*

As requested, unscaled lymphocyte activation and soluble mediator data have been included as Figure 5— figure supplement 2 and Figure 6—figure supplement 1, respectively (replacing former supplementary figures 5 and 7). In addition, updated Figure 6G panel now depicts correlation analysis with the unscaled cytokine concentrations.

> *The DosR-regulon:*
>
> *The authors hypothesize that differences in the prevalence of the dormancy metrics (acid-fastness or lipid inclusion prevalence, are due to strain-specific increases in expression of the DosR regulon within the model's hypoxic conditions (lines 107-114, 126-127). The claim that their model is equipped to evaluate dosR-dependent mycobacterial phenotypes was also previously proposed (Arbués et el., 2021) and should be tested. A comparison of the dosR-dependent gene expression of each strain in PBMC aggregates and broth culture by qRT-PCR would test this idea at a very basic level.*

We agree. Actually, a similar request was made during the revision of our first in vitro granuloma study for which such qPCR data were generated and presented in Fig. 1 D (PMID: 32069329). In addition, the work of Kapoor *et al.*, who originally developed the *in vitro* granuloma model also demonstrated the induction of most of the DosR regulated genes by qPCR (PMID: 23308269). We trust that the reviewer will agree that this does not need to be repeated.

> *The modern Beijing lineage strain L2C:*
>
> *The authors claim (Line 101-102) that the results of Figure 1 "confirm the higher virulence propensities of strains from modern lineages". From the data presented, it appears that strain L2C (Modern-Beijing) dominates the modern vs ancestral and inter/intra-lineage phenotypes of replication, dormancy, and apoptosis. Are significant differences between modern and ancestral lineages or between strains simply a facet of the distinct profile of L2C? Do the statistical differences disappear when the L2C group is excluded?*

Indeed, among the modern lineages' isolates, L2C exhibits a hypervirulent profile in terms of bacterial replication. However, the difference between modern and ancestral strains remains statistically significant when L2C is excluded from the analysis ($p = 0.002$). That is also the case when we analyze the proportion of dormant bacteria. Exclusion of L2C strain results in a

Kruskal-Wallis overall $p = 0.005$, and $p = 0.0002$ when we compare L2 vs. L3. Lastly, regarding the percentage of apoptotic macrophages, if we use L2B (instead of L2C) to compare, the difference is still significant *vs.* L1A ($p = 0.008$) although there is no longer a trend for L2A (p = 0.1).

> *"Dormancy":*
>
> *Dormancy is definitively a non-replicative state, where bacterial growth is absent. The authors' findings and claims appear to be incompatible with that definition, which they acknowledge (Lines 130-135). The lack of correlation between growth and dormancy in their model is supported with reference to Figure 2C, a Spearman's analysis of dormancy ratio with growth rate (inclusive of all strains under consideration). The figure supports a model where "dormancy" and "growth rate" are disjunct but also appears to show high "dormancy" accompanying increasing "growth" in the L2C group. How are strains able to grow if they are in a non-replicative state? Are the "growth rate" assays actually measures of survival? Are there different rates of infectivity? Are the bacteria growing cellularly in the serum-rich ECM, etc. etc? We need to see the hard CFU and Nile Red, and Auramine-O data to contextualize these findings. Alternatively, could the accumulation of inclusions in the model not be a reliable dormancy metric (Fines et al., BioRxiv [Preprint], 2023, PMID: 37609245)?*

We fully agree. The Nile red profiles are always relative and only depict the proportion of the population that has entered a dormant state. Nevertheless, dormancy can be dynamic and bacteria may swi]ly resuscitate in that model. Furthermore, and as depicted in Figure 2—figure supplement 1, despite showing an increased tendency to enter a dormant-like state, a considerable population of lineage 2 bacilli still remains metabolically active and in a replicative state. The referred preprint is very interesting and we will follow it up closely.

> *Specificity of responses to PBMC aggregation:*
>
> *The authors claim that their results "reveal a broad spectrum of granulomatous responses" (Line 73) but do not show any aggregation specificity of PBMC responses beyond the model's intrinsic metrics of area and circularity. To establish that their phenotypes such as lymphocyte activation, cytokine release, cell death, or mycobacterial acid-fastness/lipid inclusion prevalence, are aspects of the granulomatous response the authors could infect PBMCs from the same donors with the same strains and perform the same assays using established Mtb-PBMC models in which the cells do not aggregate. This would answer many important questions, for example, does the rate of macrophage infection account for variability in apoptosis percentage? Phagocytosis assay and quantification of stained intracellular mycobacteria within recently infected PBMCs could be conducted to determine if phenotypes are an aspect of granulomatous aggregation or due to strain-specific differences in cellintrinsic macrophage immunity. It would also be very informative to know what percentage of PBMCs and mycobacteria are granuloma-bound in the ECM.*

We are not aware of *Mtb*-PBMC models in which the cells do not aggregate. We previously compared PBMC infection models in the presence or absence of the collagen matrix and cells also spontaneously coalesced around infection foci (PMID: 34603299). Regarding the last point, the melting step of the collagen matrix requires enzymatic digestion and pipetting that dislocate the aggregates. Accordingly, we cannot distinguish the bacteria that would remain within the matrix compared to those replicating within cellular aggregates. However, we did resolve this question by demonstrating that the bacteria were not able to grow in the absence of cells in this culture condition (Supplementary material, PMID: 34603299)

> *Minor recommendations*

> *- The term TNF-a should be replaced with TNF throughout the manuscript.*

We acknowledge that the term TNF-a can be interchangeable with TNF. However, we chose to use the TNFα terminology to differentiate it from lymphotoxin α, which is also referred to as TNF-β.

> *- The authors cite studies conducted in murine and NHP models to support the claim that "understanding of immune protective traits in TB remains insufficient and yet dominated by data from mouse and non-human primate studies" (Lines 63-64) but ignore an abundance of data from other in vivo and in vitro models that have provided numerous valuable insights in the field of TB immunology. This line should be revised or omired.*

For us, the term “dominate” implies that these models are widely used, not that they are the only ones. Other models indeed provided additional relevant data. We are citing the lung-on-chip model of McKinney’lab and the *in vitro* granuloma model of Elkigton’s lab (line 66). We would be very happy to include more references upon further specifications even though we cannot build an extensive review here.

> *- The authors claim that their model "encompasses, with the exception of neutrophils, all immune cell types involved in TB" (Lines 67-68). To support this claim, they should provide additional references or data demonstrating that the PBMC aggregates include, eosinophils, mast cells, dendritic cells, yolk-sac-derived alveolar macrophages, and Langhan's giant cells.*

With the aim of providing a more accurate and detailed information regarding the cell types present in the model, the sentence has been reformulated as: “The model encompasses all PBMC-derived cell types involved in TB immune responses, but lacks granulocytes (i.e. neutrophils, eosinophils, basophils and mast cells)” (line 260). Noteworthy, the presence of multinucleated giant cells was reported in Kapoor’s paper describing the *in vitro* granuloma model for the first time (PMID: 23308269).

> *- As an additional note, the title can be improved and made more broadly accessible by revising the use of the acronyms CXCL9, granzyme B, and TNF-α.*

To render the title more broadly accessible we propose to replace the listed acronyms by “soluble immune mediators”, but we remain opened to more appropriate and specific suggestions.

Answers to the reviewers’ public comments

Reviewer #1:

First of all, we would like to thank the reviewers for their feedback and suggestions to improve our manuscript. To strengthen the findings of our study, we have performed and added results from IL-1b and CXCL9 blocking experiments evaluating the impact on the granulomatous response and bacterial load, respectively. In the revised version of the manuscript, while we discuss the null effect on bacterial growth of the treatment with an anti-CXCL-9 antibody and the potential reason behind it, we are now reporting a negative effect on the magnitude of granuloma formation upon neutralization of IL-1b that the correlation analysis had initially suggested.

Reviewer #2:

The revised version of our manuscript incorporates now all the points detailed in the private answers to the reviewer, including clarifications on the statistical tests performed, additional

supplementary materials to transparently disclose the raw data behind the normalization approach, as well as flow cytometry data on the immune memory status of the blood donors. In addition, and as stated in the answer to reviewer #1, to test causal relationship between some host and pathogen traits, we have now performed and provided data and interpretation of IL-1b and CXCL9 blocking experiments.

Reviewer #3:

We are thankful and concur with these constructive comments and insights. We have now consistently revisited the statistics in the figures to improve clarity and included new supplementary figures reporting the raw data that were missing in the initial version of the manuscript. In addition, and as mentioned in the answers to reviewers #1 and #2, we have now performed and added IL-1β and CXCL9 blocking experiments to test causal relationship between specific host and pathogen traits. In particular, we are now reporting a negative effect on the magnitude of granuloma formation upon neutralization of IL-1β that the correlation analysis had initially suggested.

More specifically, regarding the point that our method for bacterial collection calls into question whether all *Mtb* plated for CFU assay resided within granulomatous aggregates, we previously reported that *Mtb* growth strictly required the presence of human cells in our culture conditions (Supplementary material, Arbués *et al*, 2021, PMID: 34603299). In the presence of cells, our microscopy read-out does allow us to observe extra-cellular growth if infections are carried on beyond an 8-day limit, which we applied in the current study to exclude this particular caveat.

Concerning the apparently conflicting observation that those strains displaying an increased tendency to enter a dormant-like state are the ones exhibiting the highest replication rates, we would like to point out that a considerable population of bacilli still remains metabolically active and in a replicative state. For instance, and as depicted in Figure 2—figure supplement 1, despite showing an increased tendency to enter a dormant-like state, a considerable population of lineage 2 bacilli does remain metabolically active. Moreover, dormancy can be dynamic and bacteria may swi]ly resuscitate.

Regarding the mentioned limitations of our study that we have discussed in the revised version of our manuscript, we fully concur that PBMC-based *in vitro* granuloma models lack tissue structure as well as some important stromal and immune cellular players. Nevertheless, we and others demonstrated the particular relevance of the 3-dimensional infection approach within a matrix of collagen and fibronectin by providing mechanistical insights into *Mtb* resuscitation previously associated to treatment with various immunomodulatory drugs (Arbués *et al.*, 2020, PMID: 32069329; Tezera *et al.*, 2020, PMID: 32091388).

https://doi.org/10.7554/eLife.99062.2.sa0